UC/CLC CAMPUS EARTHQUAKE PROGRAM

Strong Earthquake Motion Estimates for Three Sites on the U.C. Riverside Campus.

R. Archuleta, UCSB
A. Elgamal, UCSD
F. Heuze, LLNL
T. Lai, UCSD
D. Lavallée, UCSB
B. Lawrence, UCR
P-C. Liu, UCSB
L. Matesic, UCLA
S. Park, UCR
M. Riemer, UCB
J. Steidl, UCSB
M. Vucetic, UCLA
J. Wagoner, LLNL
Z. Yang, UCSD

November, 2000

UCRL-ID-140522

DISCLAIMER

Work performed under the auspices of the U. S. Department of Energy by the University of California Lawrence Livermore National Laboratory under Contract W-7405-Eng-48.

PREFACE

This report was prepared under the UC/CLC Campus Earthquake Program. The project was initiated as part of the Campus-Laboratory Collaboration (CLC) Program created by the University of California Office of the President (UCOP).

The UC/CLC Campus Earthquake Program (CEP) started in March 1996, and has involved a partnership between seven campuses of the University of California - Berkeley, Davis, Los Angeles, Riverside, San Diego, Santa Barbara, Santa Cruz - and the Lawrence Livermore National Laboratory (LLNL). It is designed to estimate the effects of large earthquakes on three of those campuses. Each campus has selected a primary site to demonstrate the methods and procedures used by the CEP. The following sites have been selected: the Rivera Library at U.C. Riverside, the Thornton Hospital at U.C. San Diego, and the Engineering 1 building at U.C. Santa Barbara.

The project focuses on the estimation of strong ground motions at each critical site. These estimates are obtained by using an integrated geological, seismological, geophysical, and geotechnical approach, bringing together the unique capabilities of the campus and laboratory personnel. This project is also designed to maximize student participation. Many of the site-specific results are also applicable to risk evaluation of other sites on the respective campuses. In the future, we plan to extend the integrated studies of strong ground motion effects to other interested U.C. campuses, which are potentially at risk from large earthquakes.

To put things in perspective, the aim of the CEP is to provide University campuses with site-specific assessments of their strong earthquake motion exposure, in addition to estimates they obtain from consultants according to the state-of-the-practice, i.e. Building Codes (UBC 97, IBC 2000), and Probabilistic Seismic Hazard Analysis (PSHA). The Building Codes are highly simplified tools, while the more sophisticated PSHA is still somewhat generic in its approach because it usually draws from many earthquakes not necessarily related to the faults threatening the site under study. Eventually, both the results from the state-of-the-practice and from the CEP should be analyzed, to arrive at decisions concerning the design-basis assumptions for buildings on U.C. campuses.

This report describes how the strong ground motion estimates were obtained at U.C. Riverside, where a new seismic station was installed in July 1998. The Principal Investigator at Riverside is Professor Stephen Park.

This UC/CLC project is funded from several additional sources, which leverage the core support provided by the Office of the President and which are gratefully acknowledged. These include the University Relations Program at LLNL, formerly directed by Dr. Claire Max and presently by Dr. Harry Radousky, and the offices of the appropriate Vice-Chancellors on the various campuses. At U.C. Riverside, the Vice-Chancellor Administration is C. Michael Webster.

The Director of the UC/CLC Campus Earthquake Program is Dr. Francois Heuze from LLNL.

TABLE OF CONTENTS

Page

EXECUTIVE SUMMARY

This is the second report on the UC/CLC Campus Earthquake Program (CEP), concerning the estimation of exposure of the U.C. Riverside campus to strong earthquake motions (Phase 2 study). The first report (Phase 1), dated July 1999, covered the following topics:

- seismotectonic study of the Riverside region
- definition of causative faults threatening the UCR campus
- geophysical and geotechnical characterization of the Rivera library site
- installation of the new CEP seismic station
- and, initial acquisition of earthquake data on campus.

The main results of Phase 1 are summarized in the current report.

This document describes the studies which resulted in site-specific strong motion estimates for three sites on campus: Rivera library, Parking Lot 13 (PL 13), site of the future Physical Sciences 1 building, and Parking Lot 16 (PL 16) where the new Engineering Science 2 building is proposed for construction. The main elements of Phase 2 are:

- determining that a M 7.0 earthquake involving the San Jacinto Valley segment of the San Jacinto fault and a portion of the San Bernardino segment is the largest threat to the campus. Its recurrence interval is of the order of 100 years.
- recording numerous small earthquakes from that portion of the fault at the new UCR seismic station and at five surface campus locations in 1999.
- using the M 3.8 event recorded on March 22, 1999 as an empirical Green's functions (EGF) in scenario earthquake simulations which provided strong motion estimates (seismic syntheses) at depth of 89 m under the Rivera site, 69 m under the PL13 site, and 104 m under the PL 16 site; 120 such simulations were performed, each with the same seismic moment, but giving a broad range of motions which were analyzed for their mean and standard deviation.
- laboratory testing, at U.C. Berkeley and U.C. Los Angeles, of soil samples obtained from drilling at the UCR station site (Rivera library), to determine their response to earthquake-type loading.
- performing nonlinear soil dynamic calculations, using the soil properties determined in-situ and in the laboratory, to calculate the surface strong motions resulting from the seismic syntheses at depth.
- comparing these CEP-generated strong motion estimates to acceleration spectra based on the application of state-of-the-practice methods - the IBC 2000 code, the UBC 97 code, and Probabilistic Seismic Hazard Analysis (PSHA). This comparison will be used to formulate design-basis spectra for future buildings and retrofits at UCR.

Because of the new, site-specific approach which the CEP studies represent, an extensive effort of validation is documented on several fronts:

- validation of the EGF methodology used in the seismic syntheses of strong motions at depth
- validation of the soil profiles used for the three UCR sites
- validation of the 1-D vertical seismic wave propagation assumption for the UCR sites
- validation of the nonlinear soil models used to obtain strong motions at the surface

The ever-growing database of strong earthquake records clearly demonstrates the potential for great variability of ground motions from site to site in a given earthquake. These variations are only reflected in a coarse way in the state-of-the-practice Probabilistic Seismic Hazard Analyses, which are rather generic. They are not either described by the simplified design spectra of the Building codes (UBC 97, IBC 2000). These shortcomings provide a strong justification for augmenting the state-of-the-practice estimates with site-specific studies such as done by the Campus Earthquake Program.

At UCR, the Phase 2 studies lead to the following important conclusions:

- the motions estimated at the three UCR sites are generally comparable. Because these sites have a fairly deep (more than 60 m) soil cover over the granite bedrock, it is expected that these CEP motions will be representative of those that could be expected at other campus locations where the soil cover is in excess of say 30 m. Motions at locations with shallower bedrock could be expected to be less severe because of a smaller amplification of bedrock motions by the soil profile.
- the horizontal motions corresponding to the mean CEP estimates are at least as strong as those corresponding to the PSHA estimates for a 950-year return period event. They are significantly higher (30 to 50%) than those corresponding to the UBC 1997 or the IBC 2000 spectra.
- the Design-Basis spectrum used in the retrofit of the Rivera library is considerably lower (a factor of 2) than the CEP mean estimates, and is substantially lower than the UBC, IBC, and 475-year return PSHA event.
- the + 1 sigma CEP estimates are comparable to the estimates from a 2375-year return period PSHA analysis.
- the motions estimated by the Campus Earthquake Program are very consistent with records from recent earthquakes of comparable magnitudes in California (Hector Mine, Landers, Loma Prieta).

These results should incite a re-examination of earthquake ground motion assumptions at UCR.

LIST OF FIGURES

LIST OF TABLES

INTRODUCTION

1.1 The Campus Earthquake Program (CEP)

The approach of the CEP is to combine the substantial expertise that exists within the UC system in geology, seismology, and geotechnical engineering, to estimate the earthquake strong motion exposure of UC facilities. These estimates draw upon recent advances in hazard assessment, seismic wave propagation modeling in rocks and soils, and dynamic soil testing. The UC campuses currently chosen for application of our integrated methodology are Riverside, San Diego, and Santa Barbara. The procedure starts with the identification of possible earthquake sources in the region and the determination of the most critical fault(s) related to earthquake exposure of the campus. Combined geological, geophysical, and geotechnical studies are then conducted to characterize each campus with specific focus on the location of particular target buildings of special interest to the campus administrators. We drill and geophysically log deep boreholes next to the target structure, to provide direct in-situ measurements of subsurface material properties, and to install uphole and downhole 3-component seismic sensors capable of recording both weak and strong motions. The boreholes provide access below the soil layers, to deeper materials that have relatively high seismic shear-wave velocities. Analyses of conjugate downhole and uphole records provide a basis for optimizing the representation of the low-strain response of the sites. Earthquake rupture scenarios of identified causative faults are combined with the earthquake records and with nonlinear soil models to provide site-specific estimates of strong motions at the selected target locations. The predicted ground motions are shared with the UC consultants, so that they can be used as input to the dynamic analysis of the buildings.

Thus, for each campus targeted by the CEP project, the strong motion studies consist of two phases, Phase 1 – initial source and site characterization, drilling, geophysical logging, installation of the seismic station, and initial seismic monitoring, and Phase 2 – extended seismic monitoring, dynamic soil testing, calculation of estimated site-specific earthquake strong motions at depth and at the surface, and , where applicable, estimation of the response of selected buildings to the CEP-estimated strong motions.

1.2 Previous CEP Studies Completed at U.C. Riverside

The Phase 1 studies were completed in 1999, and are reported in details in Park et al, 1999. The main results are summarized below.

An extensive review of the seismotectonics of the Riverside region was completed. It drew heavily upon the work of the Southern California Earthquake Center (Jackson et al, 1995). The most severe seismic exposure is thought to be due to the San Jacinto Valley segment of the San Jacinto fault, at

a distance of 9 km from the campus. The maximum earthquake magnitude on this segment is estimated at M 6.9 (Petersen et al, 1996).

The seismic, geophysical and geotechnical site characterization included the following tasks:

- P and S-wave seismic refraction surveys at several campus locations
- gravity profiling, with 30 stations spanning the campus, to estimate the depth to the granite basement
- four cone-penetration tests (CPT) to depths up to 35 m, at sites surrounding the Rivera library; these included shear-wave velocity measurements.
- P and S-wave suspension logging of the 99-m deep hole at the location of the new seismic station.

These studies established that the UCR campus has a thickness of sediments (soils) overlying bedrock which may vary between 60 and 150 m, depending upon location. The seismic velocity profile of the soil column at the Rivera library is shown in Figure 1.1. The increase in the P-wave velocity without a corresponding increase in the S-wave speed shows the water table at a depth of 70 m.

Then, the new UCR seismic station was installed. It is shown in Figure 1.2. The station has three 3-component seismometers from Kinemetrics. The deepest Hyposensor is at 99.1 m in granite. An intermediate-depth Hyposensor is at 31.9 m, and there is an Episensor at the surface. These sensors are connected to two Quanterra 4128 24-bit seismic dataloggers with a total of 12 channels (3 spare channels and 9 used for the deep, shallow, and surface sensors). Timing is provided by internal clocks which are continually updated by signals from a GPS receiver mounted on the roof of Rivera Library. Both recording units are connected via real-time Ethernet links to the Trinet data center run by the USGS (http://www.trinet.org/scsn/scsn.html), and to the IGPP data center at U.C. San Diego (http://epicenter.ucsd.edu/ANZA/home.html). Currently, all sensors are telemetered. Earthquakes are digitally recorded both locally onto a disk drive at U.C. Riverside and at the Southern California Earthquake Center (SCEC) where the data are available for retrieval to all researchers via the Internet. The station became operational in August 1998.

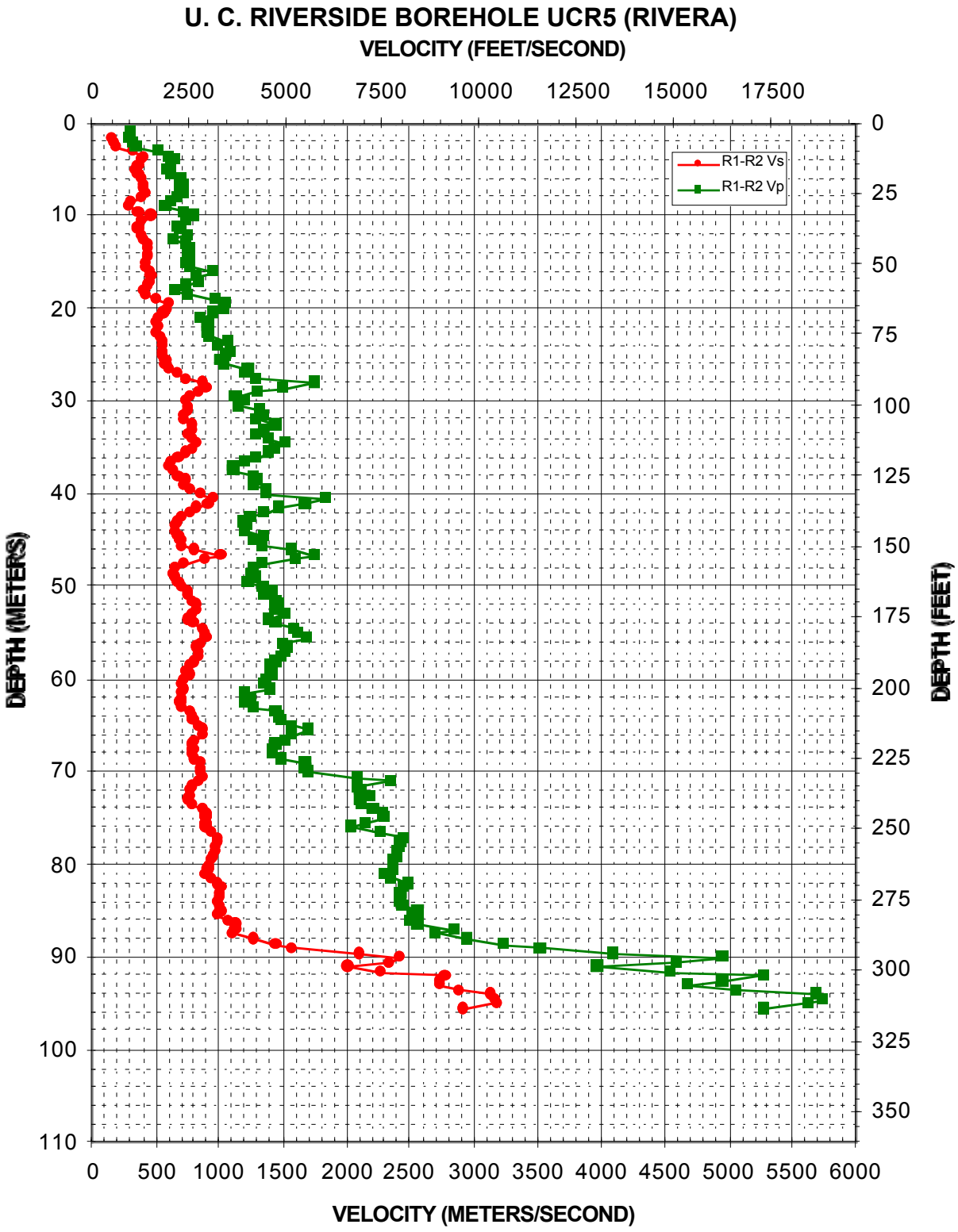

Figure 1.1: Seismic velocity profile of the Rivera site at UCR.

Figure 1.2 The new seismic station at UCR (installed August 1998). Top: surface vault (green box) on the north side of Rivera library. Bottom: inside the vault; the Episensor surface sensor is at right, and the cables from the two downhole sensors are at left. The recorders are inside the library.

2.0 NEW SEISMOLOGICAL STUDIES

2.1 New Earthquake Records

Many earthquakes have been recorded at U.C. Riverside since 1998. The data were obtained both at the Rivera seismic station and during a field deployment of surface seismometers at five campus sites, which took place between January and September 1999. These sites were numbered from 4 through 8 and are shown on Figure 2.1.

station 4: parking lot 16; west end of generator enclosure
station 5: parking lot 13; intersection of lots 10, 13, and road leading to Botanical Gardens
station 6: south-east corner of Spieth Hall
station 7: parking lot 22; east end of the island
station 8: south end of the baseball field, south of the Recreation Center

Figure 2.1 Locations of the temporary surface seismic stations deployed January-September, 1999.

The detailed records and the initial data analysis are available from U.C. Riverside's Professor Stephen Park, who supervised the field deployment. Of the 114 earthquakes recorded during that deployment, a representative sample of 27 is given in Table 2.1. It is limited to events that were located within 2.5 km from the segment of the San Jacinto fault used for the UCR seismic syntheses. The great majority of these earthquakes are very small and thus have a low signal-to-noise ratio. However, because of the quality of its signal, event 42 which was also recorded at the Rivera station on March 22, 1999 (Figure 2.2) could be used as an empirical Green's function, as discussed in section 2.2.

Table 2.1 Samples of earthquakes recorded at UCR from January through September, 1999

Event no.	Date	UTC	Lat. N	Long. W	Mag.	Stn. 4	Stn. 5	Stn. 6	Stn. 7	Stn. 8
3	99/01/21	0:03:56	34.09	117.31	2.2		5a3-39	6a1-03		
4	99/01/23	20:33:30	34.06	117.28	2.2	4a3-23				
5	99/01/23	23:54:23	33.97	117.23	2.3	4a3-24		6a1-05		
8	99/01/27	6:23:53	34.03	117.25	2.2		5a5-05	6a1-09	7a1-02	8a1-01
17	99/02/05	3:45:06			1.4			6a1-24		8a2-03
20	99/02/07	17:46:42			2.0		5a7-31	6a1-27	7a2-03	8a2-06
22	99/02/09	7:17:36	34.00	117.22	2.0			6a1-29	7a2-13	8a2-10
28	99/02/25	12:17:55	34.13	117.40	2.3		5a9-82		7a5-18	8a3-04
29	99/02/25	17:51:42	34.01	117.24	2.2				7a5-19	8a3-07
30	99/02/28	7:13:22	34.01	117.24	2.1	4a8-10	5b1-34		7a6-03	8a4-10
31	99/03/01	22:34:28	34.04	117.28	2.4	4a8-32	5b1-54		7a6-11	8a4-19
37	99/03/08	23:06:47	34.01	117.23	2.0		5b3-11	6a3-13	7a8-05	
38	99/03/11	14:20:35	33.96	117.23	2.0			6a3-53	7a8-14	8a6-05
42	**99/03/22**	**8:31:29**	**34.03**	**117.23**	**3.8**		5b4-100	6a4-28	7a9-19	8a7-05
45	99/04/07	1:59:18	34.04	117.25	2.2		5b6-35		7b2-13	
47	99/04/10	1:18:52	34.06	117.29	2.5	4b7-11	5b7-21	6a7-24	7b3-11	
55	99/04/16	16:26:06	34.02	117.24	2.1		5b8-25	6a8-69		
59	99/04/24	19:27:19	34.04	117.26	1.9		5b9-19	6a9-83	7b5-38	
63	99/05/06	0:01:52	34.09	117.32	2.2			6b1-90		8b2-14
76	99/05/25	23:12:51	34.02	117.24	1.9	4c6-07	5c8-30	6b7-30	7c4-05	8b7-02
87	99/07/01	12:08:03	34.03	117.28	2.0			6c4-24		8c3-11
90	99/07/17	1:15:28	33.97	117.23	1.5				7d3-05	8c5-05
91	99/07/17	10:37:49	34.05	117.26	1.8					8c5-06
95	99/07/25	12:28:29	33.97	117.24	1.6		5e1-06	6c7-07	7d4-09	8c6-05
100	99/08/12	12:47:47	34.05	117.26	2.1		5e6-01			
101	99/08/12	14:24:53	34.01	117.23	2.3			6d2-08		
104	99/08/16	04:25:49	34.01	117.23	1.6				7e1-06	8d1-06

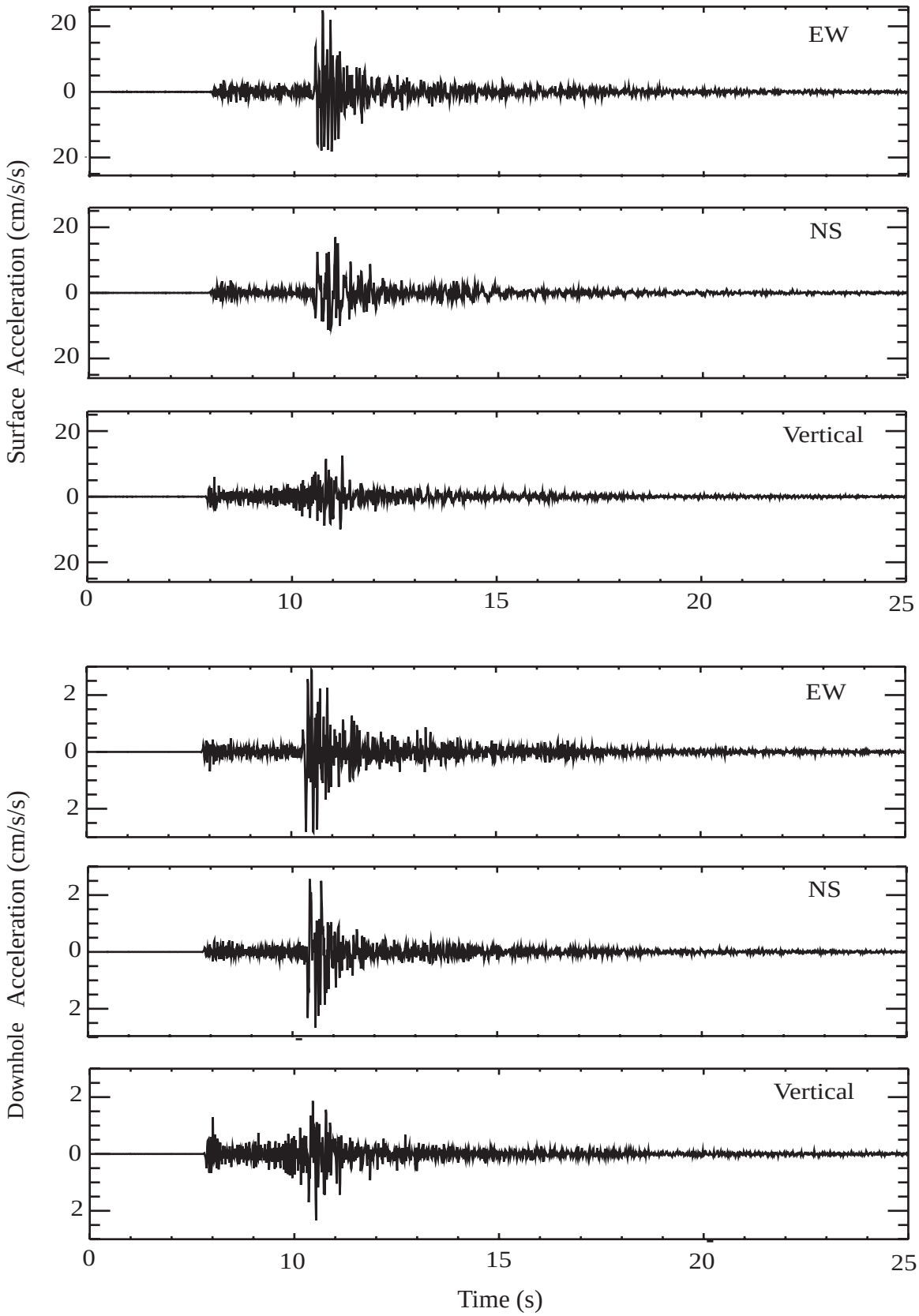

Figure 2.2 Downhole (-99m) and surface records at Rivera of the March 22, 1999 M 3.8 event.

2.2 Down-Hole Strong Motion Syntheses

2.2.1 Method

The basic principle used in the simulations is the representation theorem (e.g., see Aki and Richards, 1980). This theorem states that the ground motion observed at a location is the spatial integral over the fault plane of the temporal convolution of the source time-function with a Green's function. The source time-function may vary from point to point on the fault as can the Green's function. This is the basic method used in kinematic modeling of seismic sources. The key ingredients in this method are the specifications for the source time-function and for the Green's function.

Let us consider the Green's function. The Green's function is the response of the medium recorded by an observer due to an impulsive force applied at a point in the medium. In our case the natural location is a point on the fault plane. Green's functions can be computed numerically provided that the material properties of the medium can be specified for the entire region of interest. Of course, as one goes to higher frequencies (shorter wavelengths), knowledge of the material properties becomes more uncertain. Also, the expense of computing high-frequency Green's functions in a three-dimensional medium scales with the fourth power of the frequency. To circumvent the uncertainty in the description of the medium and the expense of computing high-frequency 3-D Green's functions, we have used an empirical Green's function (EGF) method that originated with Hartzell (1978). In the EGF method, small earthquakes recorded at the site of interest are used as if they were point sources. The primary advantage of this method is that if the source is on the fault of interest, the ray paths that are sampled by the small earthquake include the 3-D heterogeneity of the earth between the source and the observer. Thus the effects of propagation are naturally accounted for.

The empirical Green's function (EGF) method has been used extensively for deterministically synthesizing strong ground motion, as well as in inversions for parameters of the source rupture process (Hartzell, 1978; Wu, 1978; Hutchings, 1991; Tumarkin and Archuleta, 1994; Hutchings et al., 1996; Pavic et al., 2000). The primary assumption of the EGF method is that locations of small earthquakes are near the fault of the expected large event. Consequently, a small earthquake recording represents the impulse response of the path between the source and receiver. The complexity of the earthquake rupture is convolved with the Green's function to produce broadband strong ground motions. To date it has been impossible to model deterministically the detailed source process and wave propagation in such a way as to reproduce acceleration waveforms that match in both phase and amplitude for large earthquakes. However, we can avoid some of these difficulties in the estimation of strong ground motion by randomizing some source parameters and by using small earthquake recordings as empirical Green's functions (Hartzell, 1978; Wu, 1978).

The source description itself presents difficulties. The fault area has to be populated in some way with parameters that describe the kinematics of the source. There are different ways to subdivide the fault plane. In our method we grid the fault into a large number (10,000) of equal-sized subfaults. For each subfault we represent the source with three basic parameters: a stress parameter that corresponds to Brune's (1970, 1971) effective stress, a corner frequency, and a rupture time. The seismic moment is proportional to the stress parameter divided by the corner frequency cubed. The sum of all subfault moments is equal to the seismic moment of the large event. The corner frequency is inversely related to the rise time—the time it takes for the slip to reach its static value. The rupture time is the time after nucleation at which a point on the fault initiates slipping. The rupture time enforces causality of slip on the fault plane. These three parameters can be easily related to the parameters of the Haskell (1966) kinematic source description that has been the basis for numerous inversions and forward modeling efforts. The difficulty is in selecting the appropriate combination of the parameters to ensure that these parameters reflect the faulting that occurs during actual earthquakes.

Besides the seismic moment, corner frequency, and location of small event, we must specify the following input parameters for the simulated large event:

- seismic moment and corner frequency (only seismic moment if constant stress drop scaling is assumed)
- geometry of the main fault (strike, dip, length, and width) and location of the hypocenter.

Strong ground motion from the large event can be simulated by first adjusting the scaling and timing of small event records and then summing them appropriately. The Fourier amplitude at a given observer and at a given frequency for the large event $U_l(f)$ is the summation of seismograms radiated from each subfault:

$$U_l(f) = \sum_{j=1}^{N} \frac{\tilde{\sigma}_j \sqrt{A_l/N}}{M_s f_{cs}^2} \frac{R_s}{R_j} \frac{\left(f_{cs} + \mathbf{i}f\right)^2}{\left(f_{cj} + \mathbf{i}f\right)^2} U_s(f) \exp\left(-\mathbf{i}2\pi f\left(t_{sj} + t_{rj}\right)\right) \exp\left(\frac{\pi f\left(R_s - R_j\right)}{\overline{Q}\,\overline{V}_s}\right) \qquad (1)$$

Here $U_s(f)$, M_s, and f_{cs} are the Fourier amplitude at frequency *f*, seismic moment, and corner frequency of a small event, respectively. R_s/R_j is the geometrical spreading correction. $\overline{Q}$ and $\overline{V}_s$ are average values of quality factor and S-wave velocity along the path between the source and receiver. N is the number of subfaults. A_l is the area of large fault. $\tilde{\sigma}_j$ and f_{cj} are the stress parameter, that proportions to stress drop $\Delta\sigma$, and the corner frequency of the subfaults, respectively. For each subfault the seismogram is delayed by the S-wave travel time from the subfault to the receiver (t_{sj}) and the time for the rupture to propagate from the hypocenter to the subfault (t_{rj}). The source parameters t_{rj}, f_{cj}, and $\tilde{\sigma}_j$ of the subfaults are described as random variables that are constrained by the overall source properties of the large event.

The rupture time is determined by dividing the distance between the center of the subfault and the hypocenter by the rupture velocity. We assume the rupture velocity of the fault to be uniformly distributed on the interval of (0.7β, 1.0β), where β is the S-wave velocity of the material in which the fault is embedded. This assumption results in an average rupture velocity of 0.85β, which is a reasonable value.

For simplicity, the stress parameter of each subevent ($\tilde{\sigma}$) is described by the Gamma distribution. The probability density function is of the form

$$p(\tilde{\sigma}) = \gamma^2 \tilde{\sigma} \exp(-\gamma \tilde{\sigma}), \tag{2}$$

where $\gamma = 2\sqrt{1.5A_l}/M_0 f_l^2$, M_0 and f_l are the seismic moment and corner frequency of the large event, respectively. The expression of γ is derived from the high-frequency acceleration spectrum and using an ω^{-2} source model (Aki, 1967;Brune, 1970, 1971).

Through numerical tests to match Brune's ω^{-2} source model, we find that the Beta distribution,

$$p(f_c) = \frac{12}{(f_{c\max} - f_{c\min})^4}(f_c - f_{c\min})(f_{c\max} - f_c)^2, \tag{3}$$

is an appropriate probability distribution for corner frequencies (f_c) of subfaults. We assume the $f_{c\min}$ equal to f_{cl}. The $f_{c\max}$ is chosen such that the total moment of the summed subevents is the same as the moment of the large event.

The subelement stress parameter and the corner frequency are randomly selected from the distributions described by Eqs. 2 and 3, respectively. While the range of values for these parameters is documented for real earthquakes, in our models we have assumed that: 1) there is no spatial correlation for the parameters, 2) the parameters are independent of each other, and 3) the radiation pattern for all waves is isotropic. These assumptions can affect the resulting ground motion. For example, including spatial correlation could produce more coherent pulses with time-scales on the order of the correlated distance divided by the rupture velocity. The correlation length itself is a parameter that is unknown for real earthquakes. Besides the spatial correlation, there will always remain a question about the independence of the variables. One can force, a priori, a relationship between variables such as stress drop and corner frequency, but there has been no study to prescribe such a relationship.

2.2.2 Validation

The basic issue of validation is the degree to which a method produces realistic estimates of the ground motion. The measure of ground motion one uses can vary significantly. For example, one could compare computed peak values of ground motion, such as peak acceleration or peak velocity, with those obtained from a specific earthquake. Other comparisons might be between the complete

time-histories in phase and amplitude or perhaps between response spectra at different periods. Each measure can be evaluated on an earthquake-by-earthquake basis.

A critical measure for our method is whether the simulated spectrum approximates the Fourier amplitude spectrum of large earthquakes (Aki, 1967,Brune, 1970, 1971) because we have assumed (based on numerous studies) that a large earthquake has a Fourier amplitude displacement spectrum which has a characteristic shape, often referred to as ω^{-2} spectrum. In Figure 2.3 we compare the results of our simulation with Brune's ω^{-2} spectrum. For the entire frequency range the kinematic source spectrum agrees with Brune's ω^{-2} spectrum. We performed several tests using a different number of subevents: the kinematic modeling results are almost independent of the number of subevents when that number is greater than 3000.

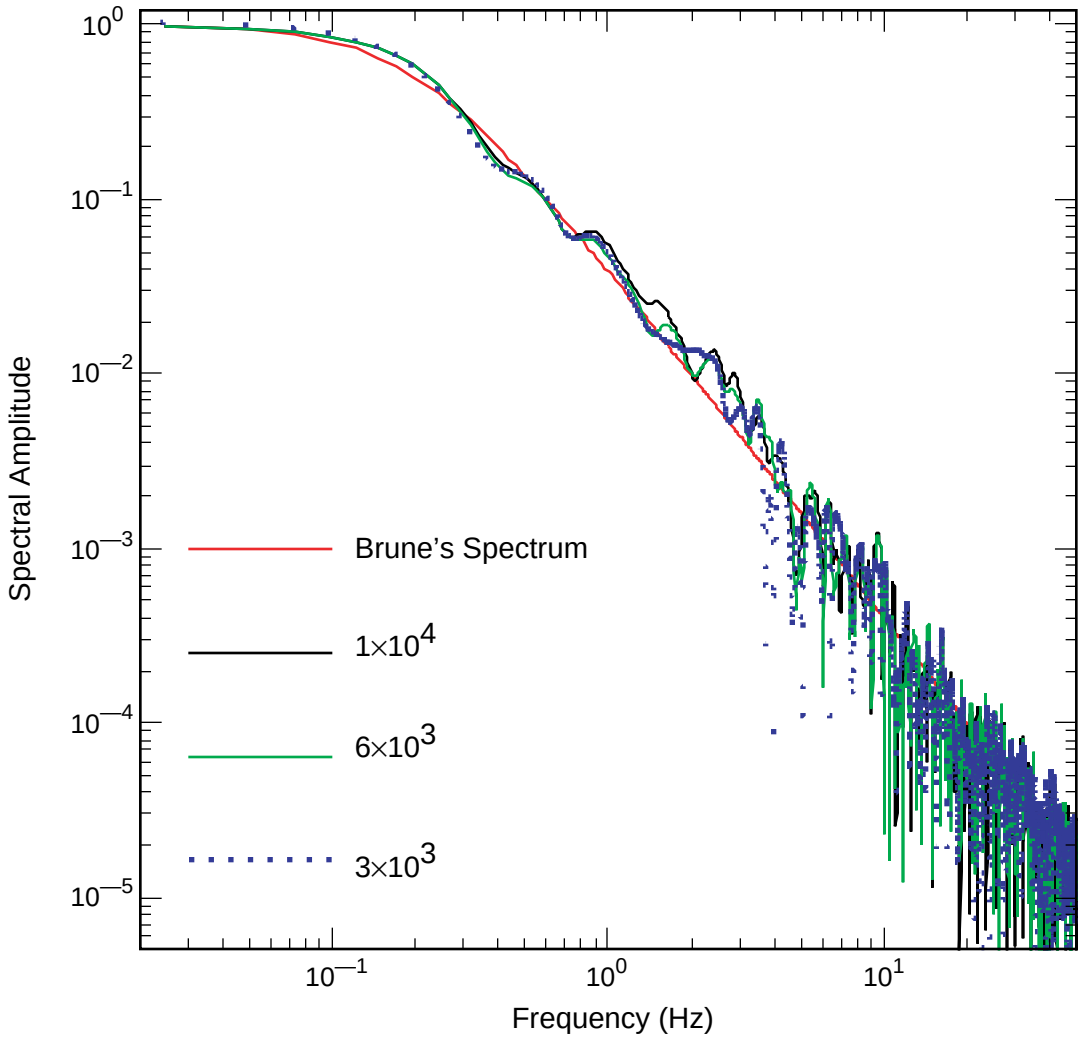

Figure 2.3 Comparison of Brune's spectrum with stochastic simulations. The corner frequency is 0.5 Hz. We separately used 3,000, 6,000, and 10,000 subevents to simulate the Brune's spectrum.

Another measure is the basic shape and level of ground motion, as compared to that predicted by probabilistic seismic hazard analysis. The probabilistic method represents an average of ground motions from a suite of different earthquakes for the same distance and magnitude as that simulated by the stochastic method. As shown later in this report, the shape and level of the synthetic response spectra agree with the probabilistic ground motions over a broad frequency range.

As a further assessment, we illustrate how an ensemble of synthetic ground motions based on the method described above can be compared with data, by using response spectra from the 1994 Northridge earthquake. We take the fault plane and hypocenter, as known. We use two well-recorded aftershocks as EGF's. For each EGF we compute 150 synthetic (linear) time-histories of acceleration from which we calculate the mean response spectrum and its standard deviation. Examples of the response spectra at three stations: Canoga Park (CPC), Santa Susana (SSA) and Moorpark (MPK) are shown in Figures 2.4, 2.5, and 2.6, respectively. The closest distance to the fault is 15.7 km, 18.1 and 26.4 km for Canoga Park, Santa Susana, and Moorpark, respectively. Canoga Park and Moorpark are alluvial sites; Santa Susana is a sandstone rock site. All three components of motion are shown. The solid line is the spectrum of the Northridge record, and the dashed lines represent the ± one standard deviation (sigma) of our estimates. Overall, the range of ground motion in the synthetics reflects the general shape of the response spectra from the Northridge earthquake.

We estimate the modeling error using the computed ground motion for the Northridge earthquake. Our model is a stochastic one that involves a convolution of an EGF with a stochastic source description. The source model parameters are the seismic moment of the mainshock, the corner frequency of the mainshock, the average rupture velocity, the fault geometry, and the hypocenter. The EGF is also part of the model in that it represents the wave propagation from source to receiver. Thus uncertainties in the model include the EGF. The output of the model, e.g., average response spectrum, average peak acceleration, average peak particle velocity, are obtained only after 150 stochastic source models have been simulated. For Northridge we fixed the source parameters and used two different EGF's. To compute the modeling standard deviation we compare the observed and computed average response spectra at seven stations. The standard deviation is computed for the period range of 0.05–2.0 s. The natural log of the standard deviation is 0.4. This modeling error is consistent with modeling standard deviation (natural log) of 0.5 found by Hartzell et al. (1996, Figure 9B) but less than the average standard deviation–about 0.8 natural log units–determined from six different methods for the 1988 Saguenay earthquake (Abrahamson and Becker, 1999).

There are differences between simulations using the two different aftershocks as EGFs, as will also be evident in the synthetics generated for UCSB. These differences reflect modeling uncertainty due to the selection of the EGF. Dan et al. (1990) found using 17 EGF's to simulate a M 6.7 event

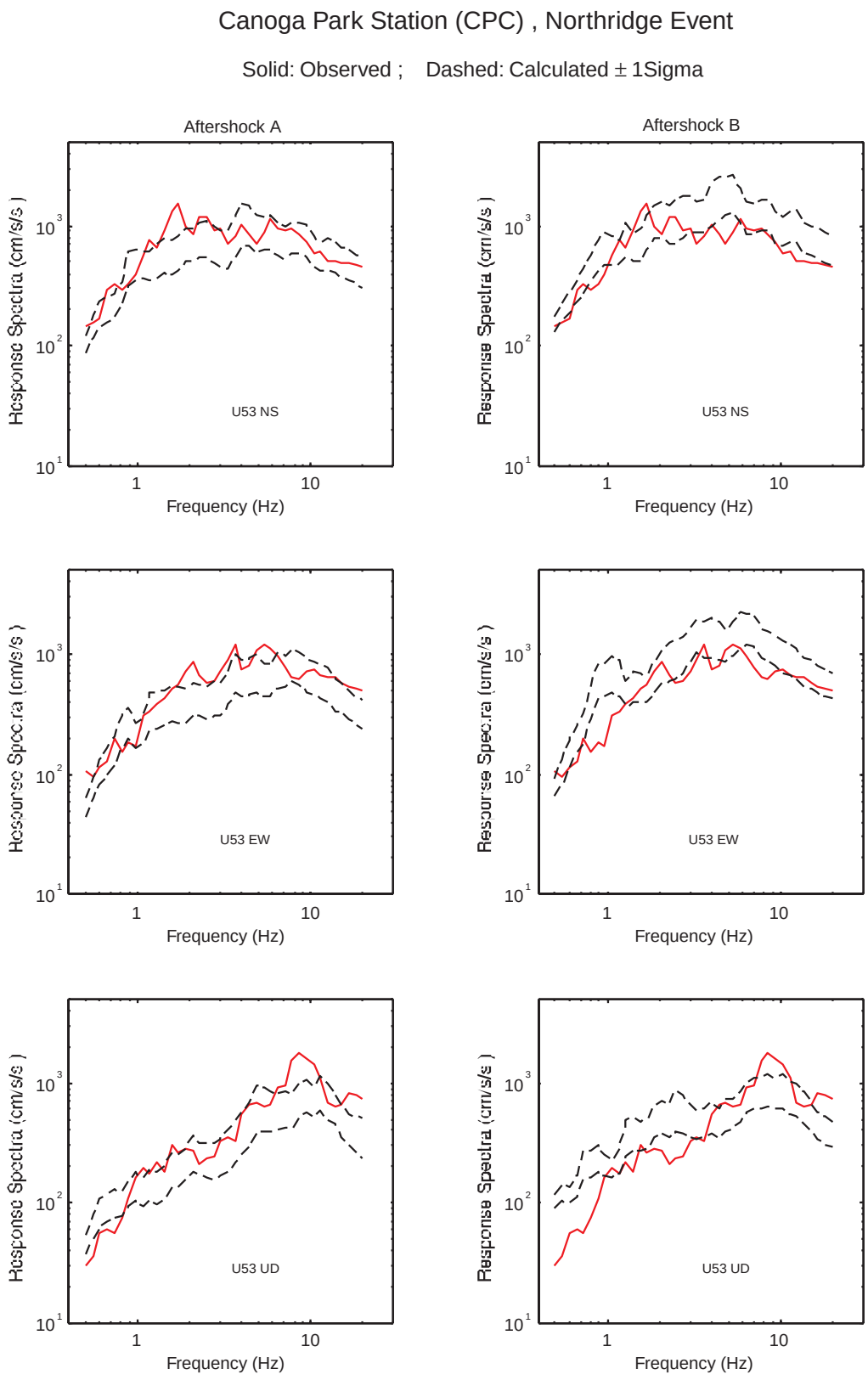

Figure 2.4 Comparison of observed and calculated spectra for Northridge records at CPC station.

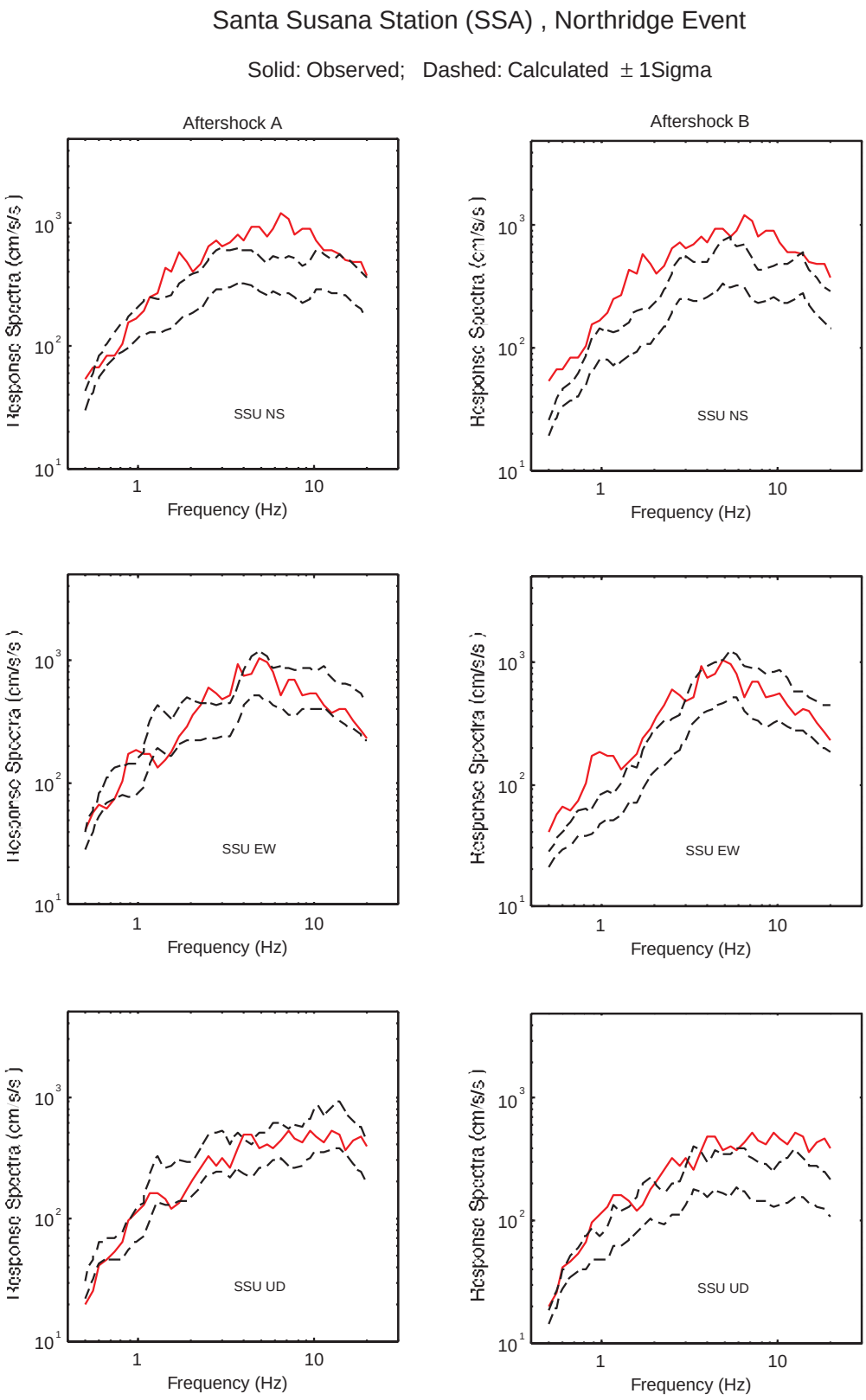

Figure 2.5 Comparison of observed and calculated spectra for Northridge records at SSA station.

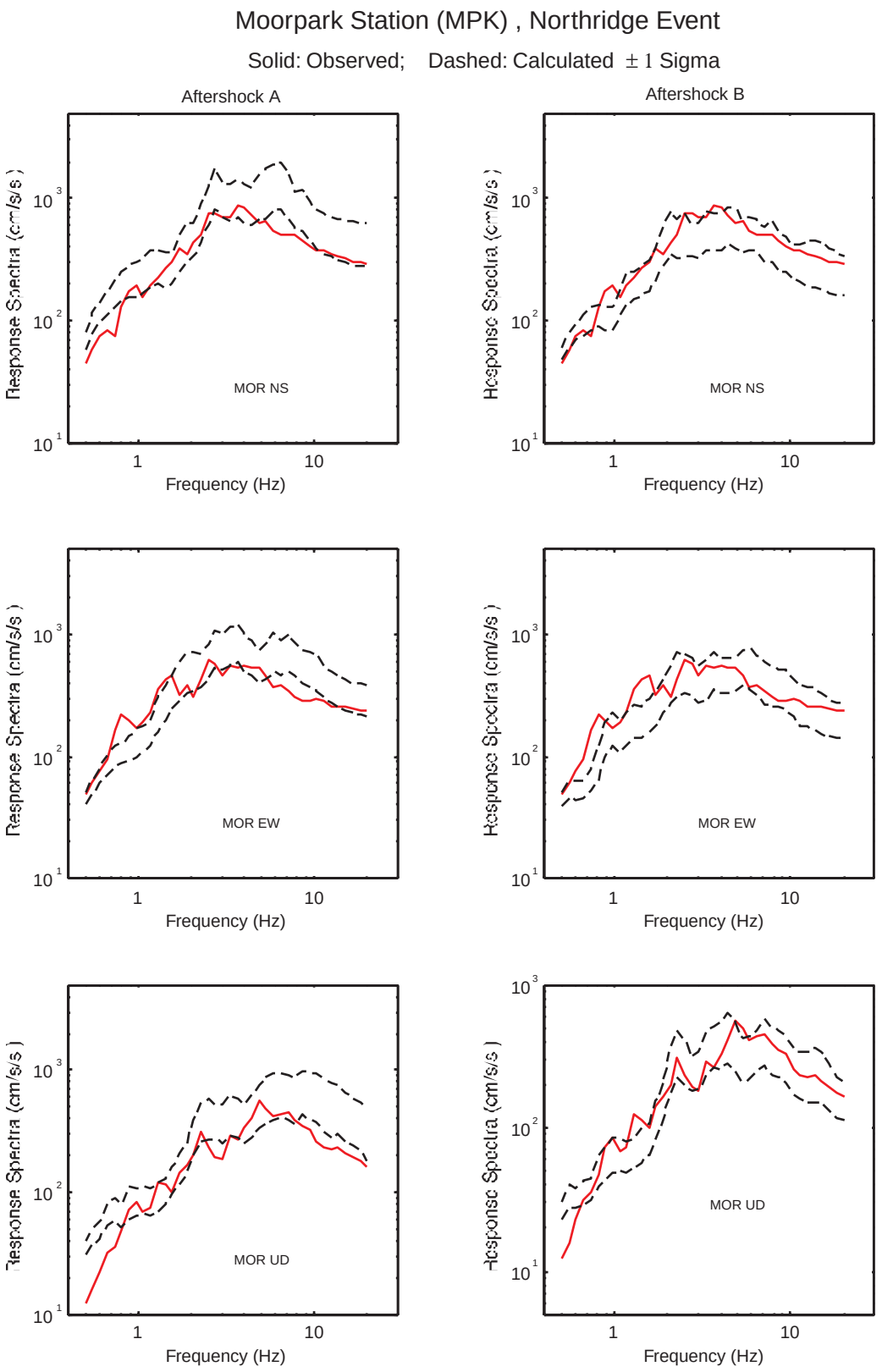

Figure 2.6 Comparison of observed and calculated spectra for Northridge records at MPK station.

(JMA magnitude) that the standard deviation was about 45%. They also found that combining all 17 EGF's into a single computation reduced the coefficient of variation to about 15% but systematically underpredicted the peak acceleration, peak velocity and spectral intensity by 12%, 11% and 19%, respectively. Jarpe and Kasameyer (1996) used EGF's to simulate ground motion at different stations for the Loma Prieta earthquake. Each of the stations had a different numbers of EGF's available to be used in the synthesis. They found no correlation between the standard error and the number of EGF's used to simulate the ground motion.

2.2.3 Fault Rupture Scenarios for the San Jacinto Fault Zone (SJFZ)

As discussed in the U.C. Riverside Phase 1 CEP report (Park et al., 1999) the range of magnitudes for an event on the SJFZ is 6.7 to 7.6. The shortest distance from the Riverside campus to the trace of the fault is about 9 km. For the San Jacinto Valley segment only, a magnitude 6.7 was estimated by Jackson et al. (1995). The retrofit of the Rivera library was based on a Maximum Credible Earthquake with M 6.9 on the San Jacinto Valley segment (CHJ Inc., 1997). Our examination of the SJFZ concluded that a realistic threat to UCR would be from a rupture of the San Jacinto Valley segment and a portion of the San Bernardino Valley segment, over a total length of 58 km. The corresponding moment magnitude is 7.0. The recurrence intervals for the two fault segments are 83 years and 100 years, respectively (Jackson et al., 1995). Accordingly, the recurrence interval for the CEP scenarios is of the order of 100 years if the rupture of one segment carries into a portion of the other segment. The activation of more than one fault zone segment has been recently demonstrated in Southern California during both the Landers and Hector Mine earthquakes. The last strong earthquake on the San Jacinto Valley segment was a M 6. 8 event in 1918.

We use a fault model with a strike of 319^{o} and a dip of 85^{o} to the northeast. The fault plane measures 58 km in length and extends from a depth of 0.5 km to 14.4 km with a down-dipping width of 14 km. The two shallowest corners of the fault plane are at 34.167^{0}N, 117.417^{0}W and 34.767^{0}N, 117.000^{0}W. The fault parameters and geometry relative to UCR are shown in Figure 2.7.

We assume that the fault rupture initiates at some point on the fault (the hypocenter) and proceeds outward along the fault surface. Because the position of the hypocenter for any earthquake cannot be reliably predicted, we chose 6 possible hypocenters as shown in Figure 2.8.

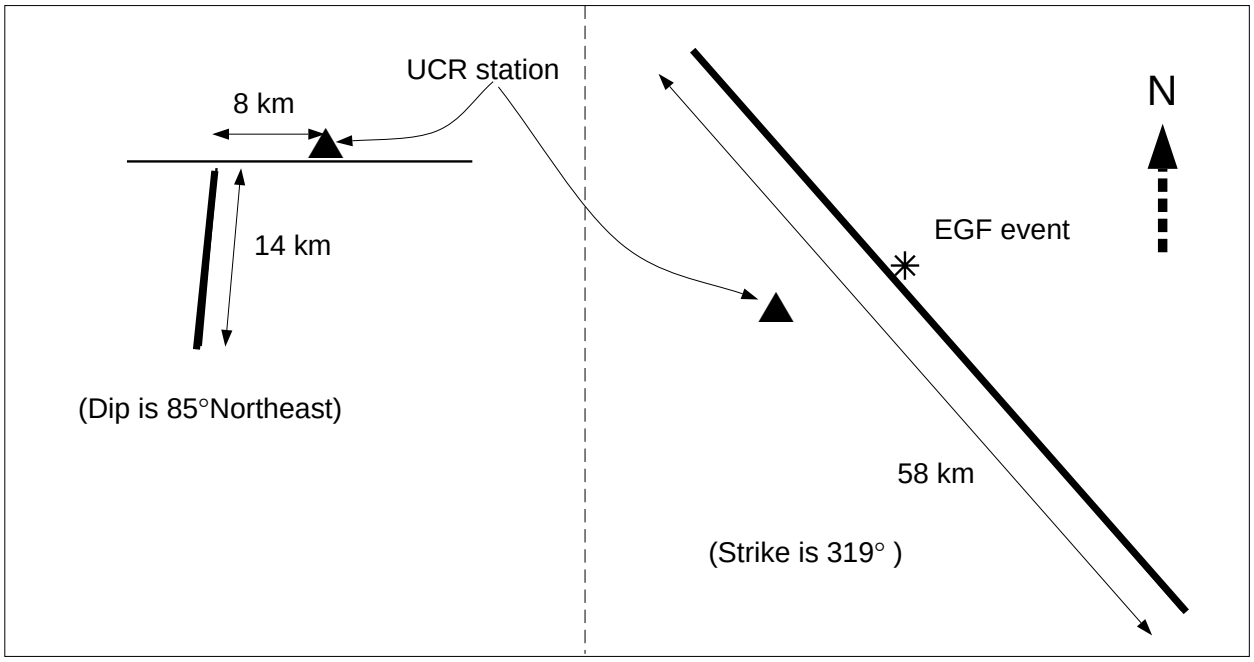

Figure 2.7 Schematic view of the scenario earthquake fault and its relation to UCR. Cross-section shown on left, and plan view on right.

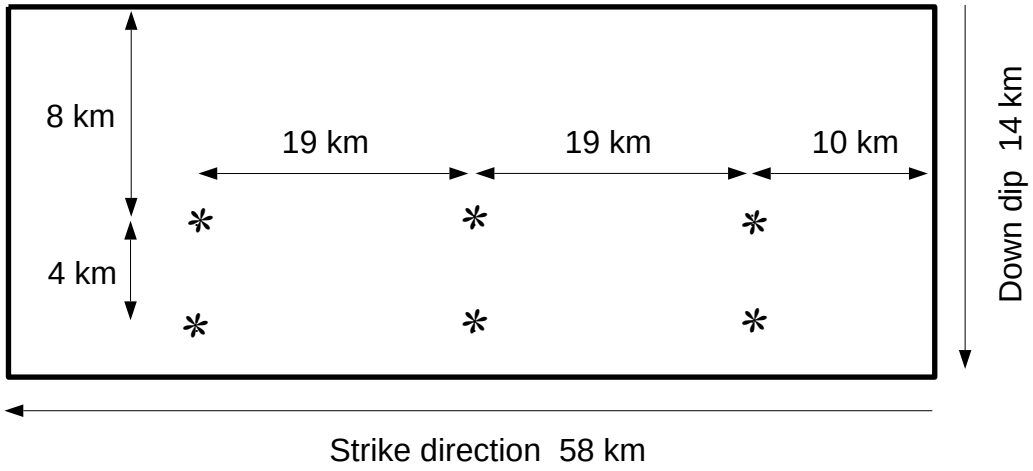

Figure 2.8 Location of 6 assumed hypocenters (star symbols) on the fault surface.

2.2.4 Downhole Strong Motion Estimates (Stochastic Syntheses)

The fault plane of the scenario earthquake is divided into 10,000 square subfaults such that the time difference between arrivals from the adjacent subfaults is less than the periods of interest. The corner frequency (f_c) of the scenario earthquake is estimated in the range of 0.08 Hz to 0.12 Hz,

with an average value of 0.10 Hz. The seismic moment (M_0) of a M_W 7.0 earthquake is 3.6×10^{26} dyne-cm.

The UCR/CEP borehole seismic station, at 33.973^0N, 117.327^0W, recorded the ground motions of one small earthquake (March 22, 1999) which occurred on San Jacinto fault and has a reported magnitude of 3.8. This event locates at 34.02^0N, 117.25^0W with a depth of 16.7 km. The recordings of this event was sampled at 100 samples per second (s/s). They are used as empirical Green's functions in our ground-motion estimation. The empirical Green's functions are band-pass filtered (Butterworth, four poles) with the corner frequencies at 0.5 and 20 Hz, to remove the low- and high-frequency noise in these recordings.

Based on Brune's ω^{-2} source model, we have calculated the seismic moment of the small earthquake directly from the long-period levels of the S-wave displacement spectra, using an average radiation pattern coefficient of 0.6. The seismic moment is 1.1×10^{21} dyne-cm. The corner frequency of the small event of 9 Hz is also estimated from the spectra.

We calculated 20 scenario earthquake for each hypocenter location giving a total of 120 three-component time-histories for a M 7.0 event on the San Jacinto fault. Because we used the surface records of the small event as our EGF, the resulting seismic syntheses were for surface motions.

Using the well-characterized soil profile of the UCR station sites, these time histories were then linearly deconvolved to a depth of -89m. This deconvolution provided the downhole incident motions. The acceleration response spectra of these downhole incident motions are shown in Figure 2.9 to 2.11, which include the mean and the +/- one sigma range. Note the substantial difference between the EW and NS directions, which reflects the influence of the directionality of fault rupture on the ground motions on campus.

The estimated mean and standard deviations for the peak acceleration of downhole incident time histories are listed in Table 2.2. For these time histories we determined a standard deviation (natural log units) of 0.32 for the response spectra averaged over the passband 0.5–20 Hz. The total uncertainty—modeling plus parameterization—of the response spectra is the square root of the sum of the variance due to parameterization (0.2025) plus the variance due to modeling (0.102). The total standard deviation is 0.55 (natural log units) averaged over 0.5–20 Hz; the mean plus one standard deviation response spectrum is 83% larger than the mean.

Table 2-2. Statistics of downhole synthesized incident peak accelerations (g)

Component	EW	NS	UP
Mean Value	0.1522	0.2073	0.1065
Standard Deviation	0.0566	0.0614	0.0339

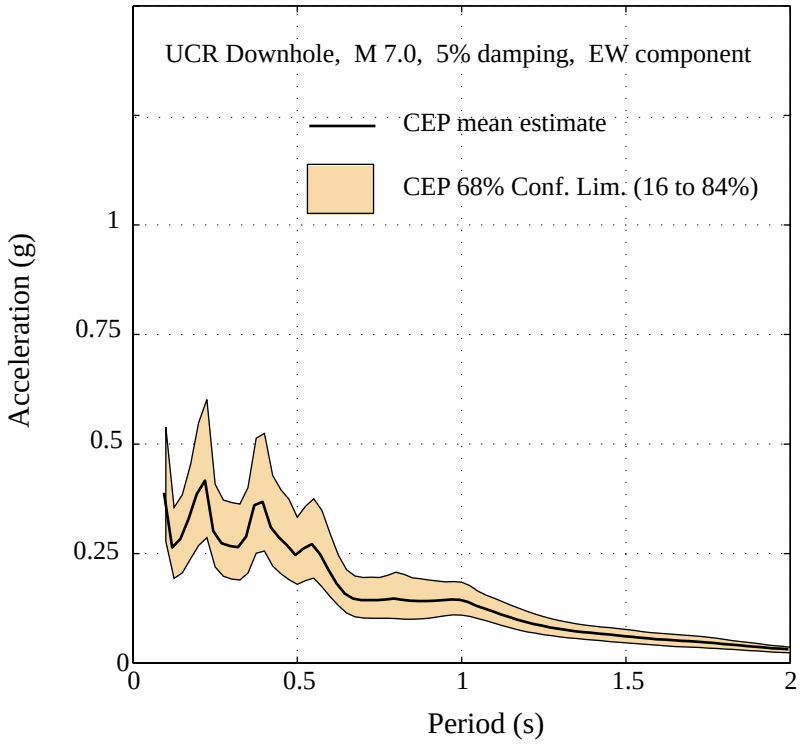

Figure 2.9 Acceleration spectra of bedrock incident motion, EW component

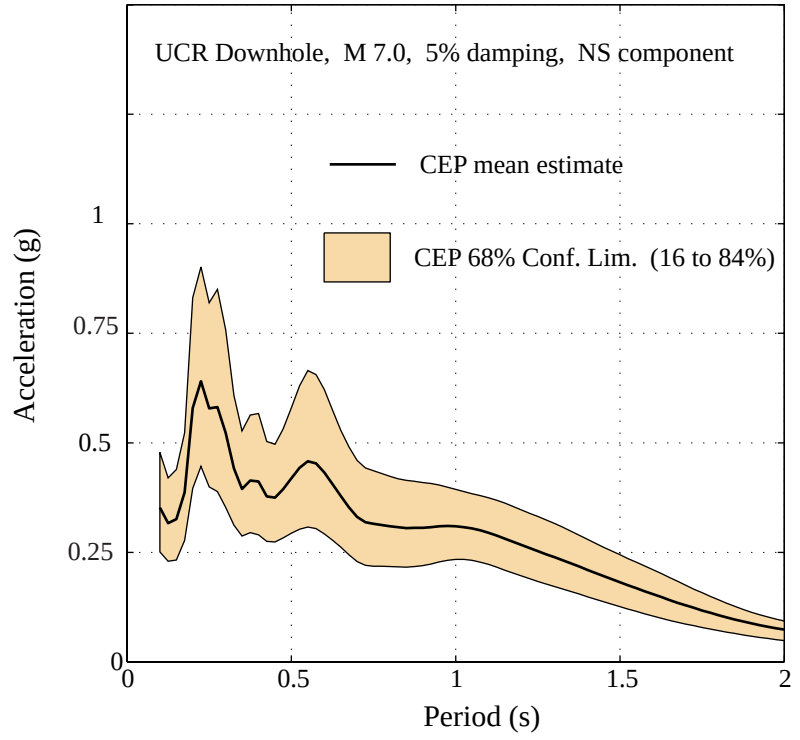

Figure 2.10 Acceleration spectra of bedrock incident motion, NS direction

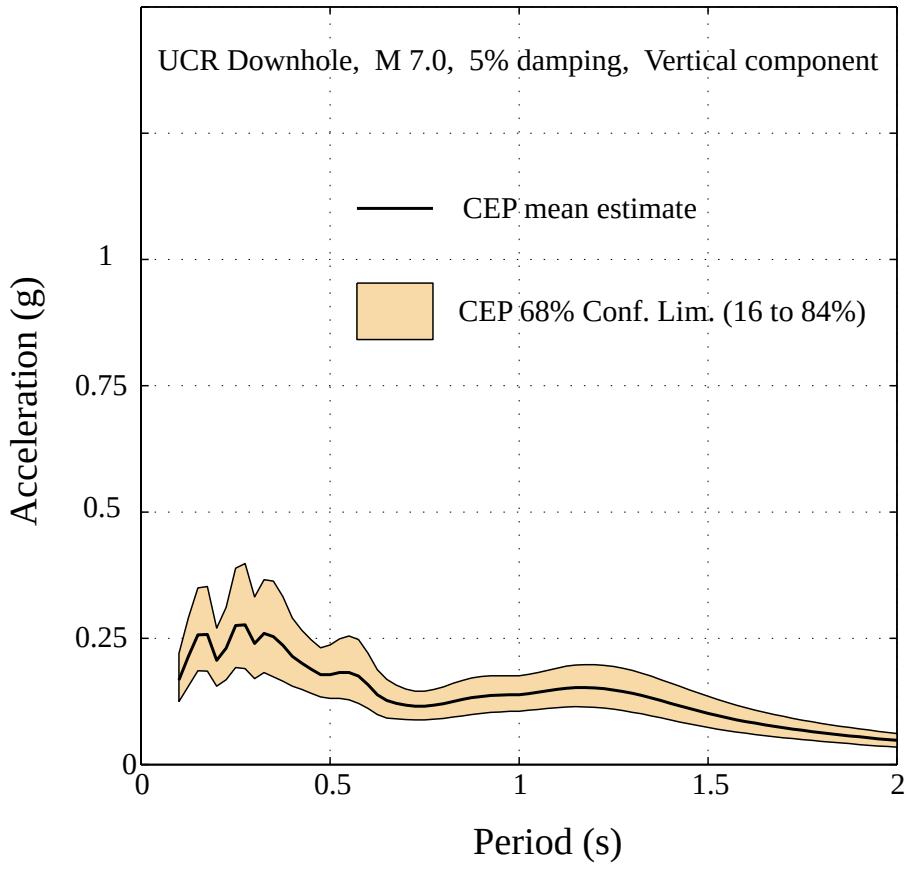

Figure 2.11 Acceleration spectra of bedrock incident motion, vertical direction

To represent the suite of time-histories we find two particular time-histories among the 120 synthetics such that their response spectra best fit the overall mean and mean plus one standard deviation. They are shown in Figure 2.12.

The stratigraphy at UCR is essentially that of alluvium resting on a basement of competent granite. For that reason, the incident motions in bedrock are assumed to be the same at all locations under the UCR campus. The variability of surface motions is due to the variability of the depth of soils overlying the bedrock.

To estimate surface ground motions, the set of 120 incident time histories are propagated to the surface, through the soil column with a nonlinear dynamic soil response code (section 4.3.1).

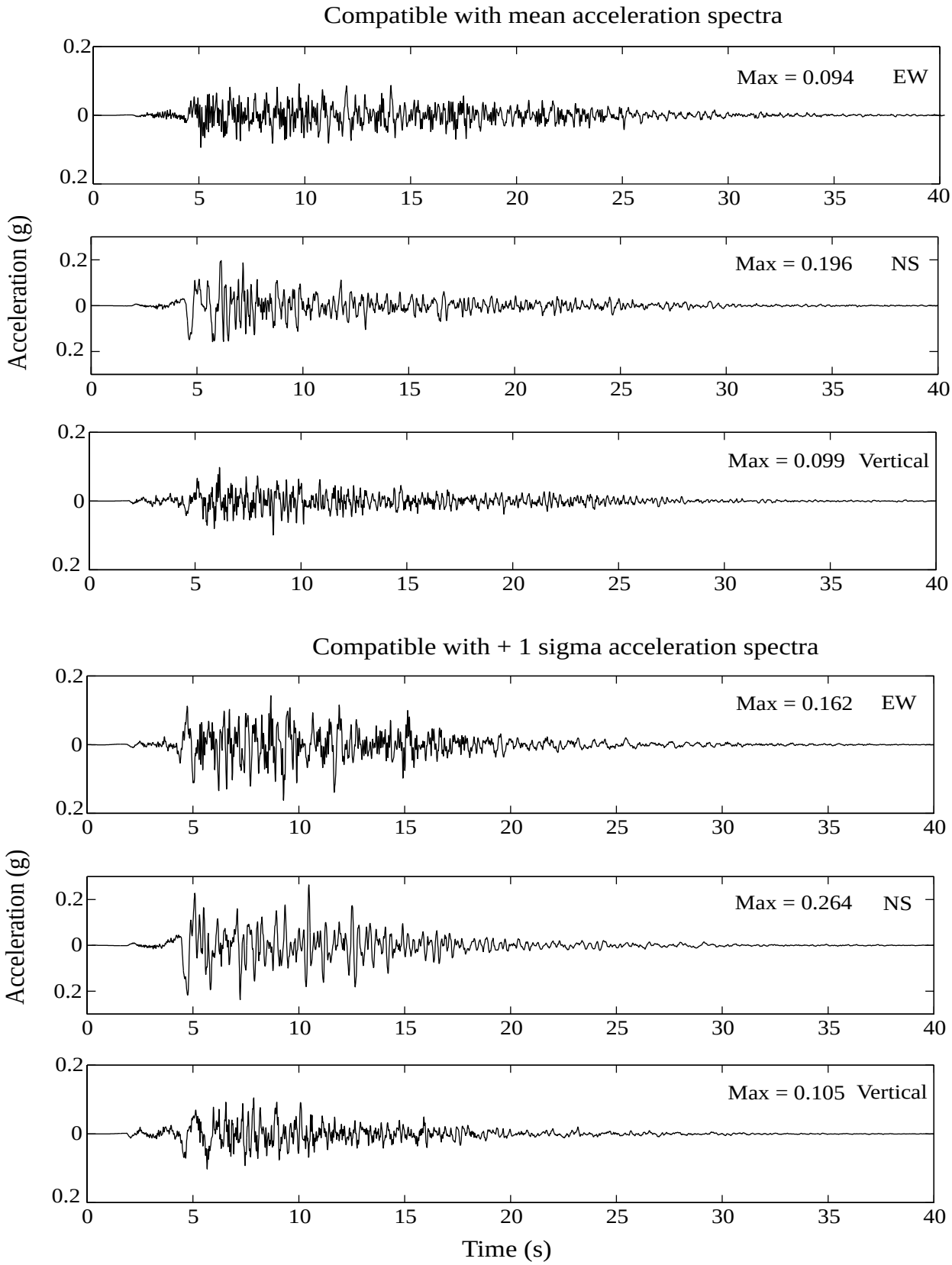

Figure 2.12 Representative incident acceleration time-histories at bedrock.

3.0 NEW DRILLING AND GEOPHYSICAL LOGGING

2.1 Logs of the New Holes at PL 13 and PL 16

Two new deep holes were drilled to bedrock at the location of future buildings: one in Parking Lot 13, site of the future Physical Sciences 1 building , and one in Parking lot 16, where the new Engineering Science 2 building is proposed for construction. As was done in Phase 1 for the Rivera site, each hole was logged with P- and S-wave suspension tools (by Geovision Inc., of Corona, CA), and with gamma and resistivity tools (by Welenco, of Bakersfield, CA). Coupled with the extensive site characterization at Rivera, these logs provided a detailed definition of the soil column and gave the necessary information to build soil dynamics models which could then be used to obtain surface strong motion estimates at these two locations, by propagating upward the bedrock strong motions determined as discussed in Chapter 2.

The elevations above sea level of the collars of the three deep holes drilled so far are: 323.6 m at Rivera, 325.1 m at PL 13, and 321.2 m at PL16.

The new P and S-wave velocity profiles are shown in Figures 3.1 and 3.2 which are at he same scale as Figure 1.1. The water table shows clearly at a depth of 59 m at PL 13 and at 71 m at PL 16. As was the case at Rivera, the ground motion relevant to seismic input to building design can be considered to be effectively in dry soils.

2.2 Comparison of the Velocity Logs at the Three Sites

A comparison of the velocity logs at the three sites reveals the following features:

- the Rivera and PL 16 velocities are remarkably similar down to 88 m. The water table depth (71 m) is identical at both places. Bedrock is deeper by about14 m at PL 16.
- the velocities at PL 13 and PL 16 are quite similar down to 22 m, and between 30 m and 66 m. The transition to bedrock is markedly shallower at PL 13 than at PL 16, 67 m vs. 103 m. This is to be expected as PL 13 is closer to the granite outcrop east of campus.
- however, the bedrock depths at the two new sites are greater than what would be expected from a linear depth interpolation between Rivera and the outcrop, i. e. assuming a constant slope of the bedrock interface. This shows that the determination of depth to granite at other locations on campus is better performed by drilling to the bedrock rather than trying to interpolate or extrapolate between known sites. The incremental cost of such drilling and logging is small compared to the initial investment at Rivera, and it enables one to confidently use the downhole seismic syntheses from Rivera as input to calculations of surface strong motions at new sites.

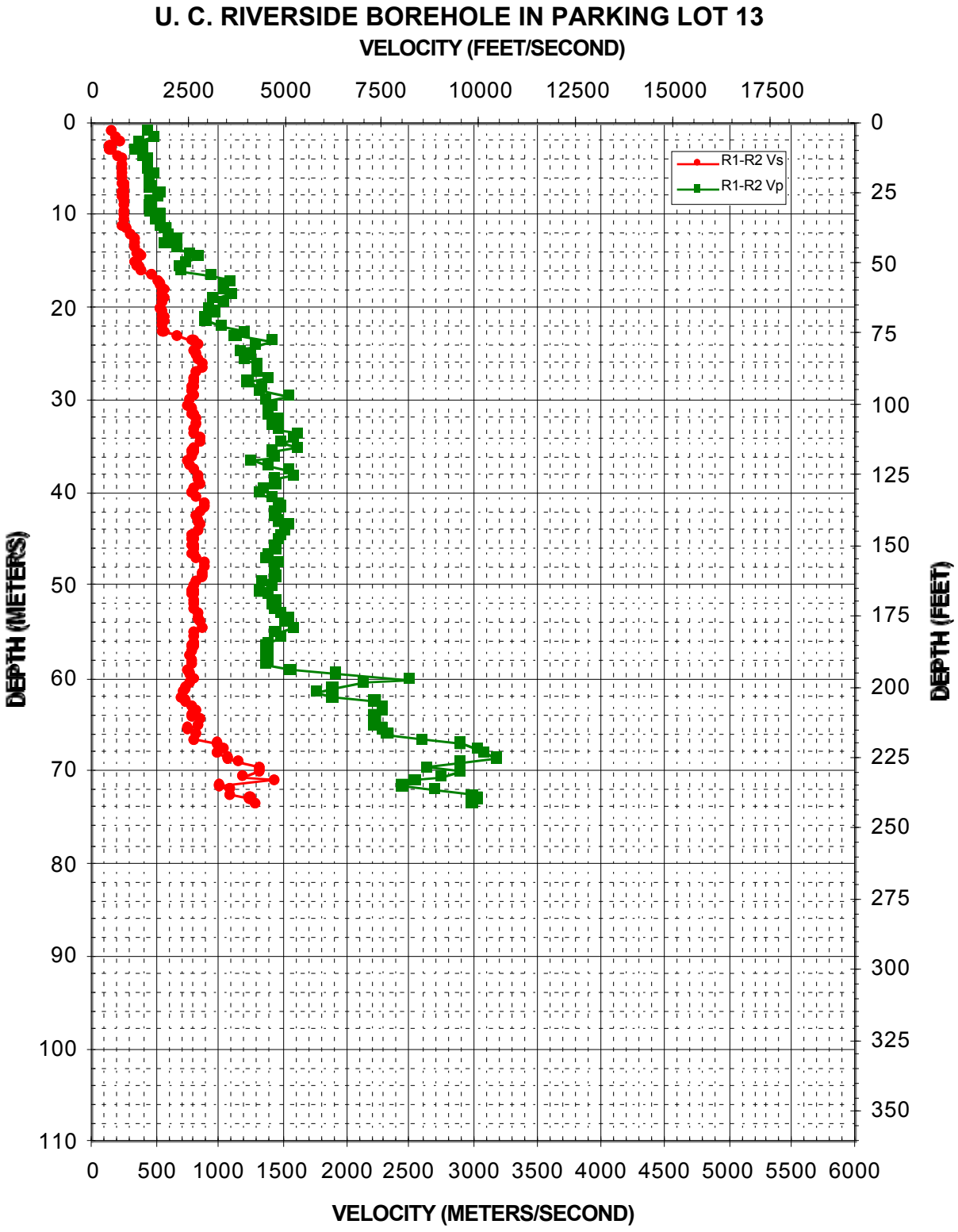

Figure 3.1 P- and S-wave velocity profiles at Parking Lot 13

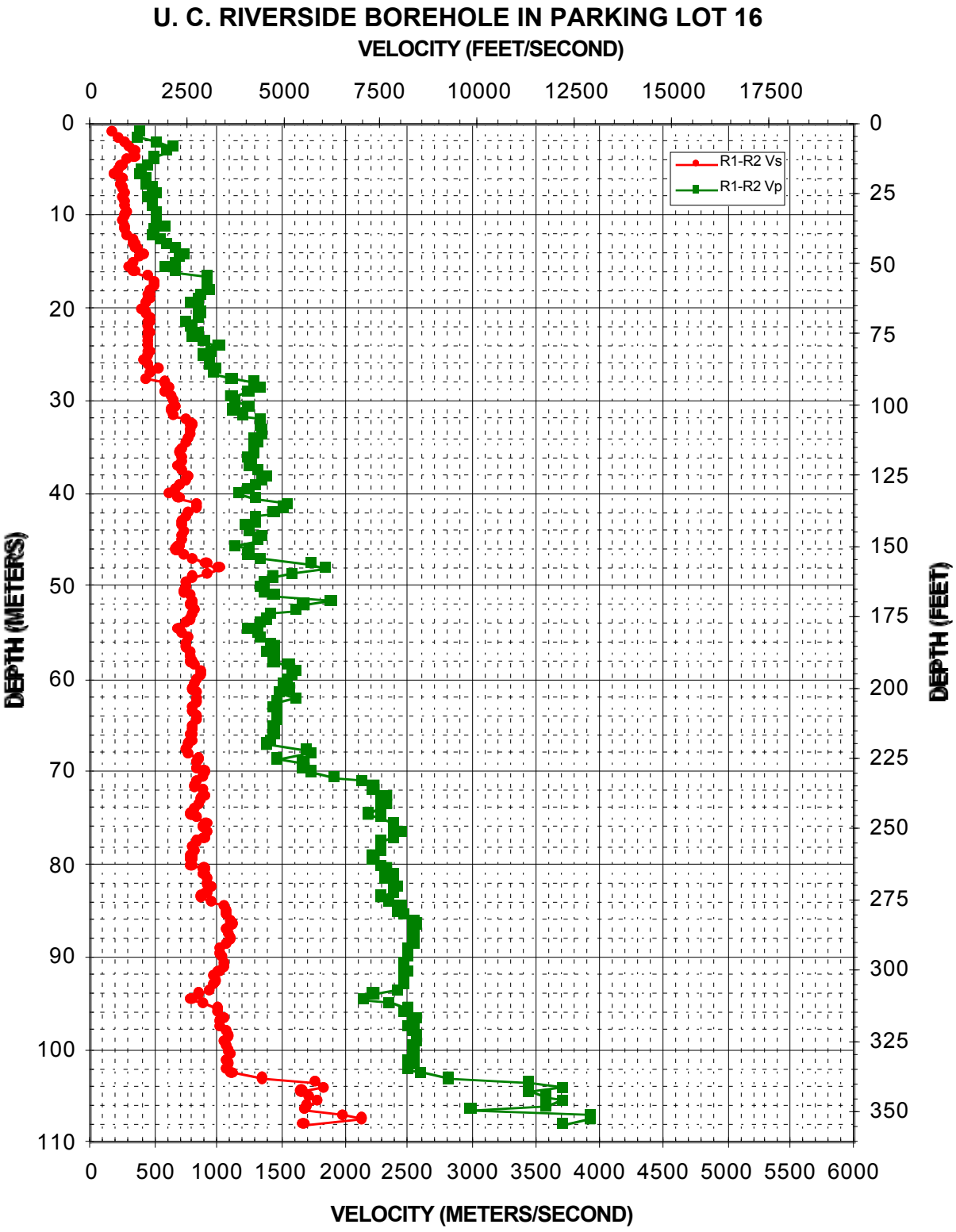

Figure 3.2 P- and S-wave velocity profiles at Parking Lot 16.

4.0 SOIL DYNAMICS STUDIES

4.1 Laboratory Tests on UCR Soils

Soil samples were recovered by Shelby tubes at the location of the seismic station. In order to complement the in-situ characterization tests and to obtain properties required for soil dynamics calculations, laboratory tests were performed on the samples. Soil classification and cyclic simple shear tests were conducted at the University of California at Los Angeles (UCLA), and monotonic triaxial tests were done at the University of California at Berkeley (UCB). The detailed test results are presented in Matesic and Vucetic (1999), and in Riemer and Abu-Safaqah (1999), respectively. Only a summary is given here. Table 4.1 shows the sample inventory and plan of tests

Table 4.1 Inventory and test plan for the soil samples from the UCR Rivera site

Tube		Depth [m]	Sample recovery length [cm]	Field visual description of soil	Delivered to U.C. Berkeley		Remained at UCLA	
No.	Label				Length [cm]	Triaxial tests planned	Length [cm]	DSDSS tests planned
1	P-1	1.5 - 2.25	46	silty sand fill with some large pieces of gravel (up to 1 inch in diameter) at the top; silty sand with pieces of gravel at the bottom; dark yellowish brown	20	1	25	1
2	P-2	3.0 - 3.75	56	silty sand (with some grains up to 0.2 inches); dark yellowish brown	28	1	28	1
3	P-3	8.85 - 9.60	46	silty coarse sand**;** with pieces of gravel (up to 0.7 inches); yellowish brown	20	1	25	1
4	P-4	11.45 - 18.3	36	silty coarse sand; yellowish brown	18	1	18	1
5	P-5	23.8 – 24.55	30	silty coarse sand; yellowish brown	0	0	30	1
6	P-6	27.1 – 27.9	27	silty coarse sand; yellowish brown	26	1	0	0
7	P-7	31.7 – 32.5	33	silty coarse sand; yellowish brown	18	1	15	1
8	P-8	36.6 – 34.75	69	silty coarse sand; yellowish brown	20	1	47	1

4.1.1 Basic Soil Properties and Soil Classification

The results of basic and soil classification tests done at UCLA are summarized in Table 4.2.

Table 4.2 Basic properties and Classification of soils from the UCR/Rivera site

Sample label	Depth (m)	LL*	PI*	Soil Classification	Dry Unit Weight (KN/m^3)	Water Content (%)	Void Ratio	Saturation of test samples (%)
P-1	2.1	#	0.0	SM – silty sand	16.9	9.3	0.60	42.7
P-2	3.7	#	0.0	SW-=SM, well-graded sand to silty sand	17.1	16.4	0.61	75.0
P-3	9.5	#	0.0	SM – silty sand	17.1	9.2	0.58	43.7
P-4	18.1	#	0.0	SW-SM, well-graded sand to silty sand	17.5	11.9	0.54	60.3
P-5	24.4	26.6	8.2	SC – clayey sand	17.8	12.0	0.54	62.6
P-7	32.3	28.4	8.0	SC – clayey sand	19.1	12.4	0.44	79.7
P-8	37.2	#	0.0	SM – silty sand	16.5	20.7	0.63	90.5

* LL : Liquid Limit PI : Plasticity Index

4.1.2 Cyclic Simple Shear Tests

These tests were conducted in the Civil Engineering Department at UCLA. The device used was designed by Doroudian and Vucetic (1995). As shown in Figure 4.1, its most unique feature is that two parallel specimens of the same soil are tested simultaneously. Such a special configuration enables almost complete elimination of problems associated with false deformation, system compliance, and friction. As a result, very small strains can be applied and measured in a controlled manner, as well as the resulting stresses. The cyclic response of the soil samples is recorded in terms of the variation of shear stress vs. shear strain over numerous cycles of loading with increasing strain amplitude. From these records one can describe the progressive decay of soil shear modulus (G) and the increase in the equivalent viscous damping ratio (λ). The definitions of these quantities are illustrated in Figures 4.2 and 4.3.

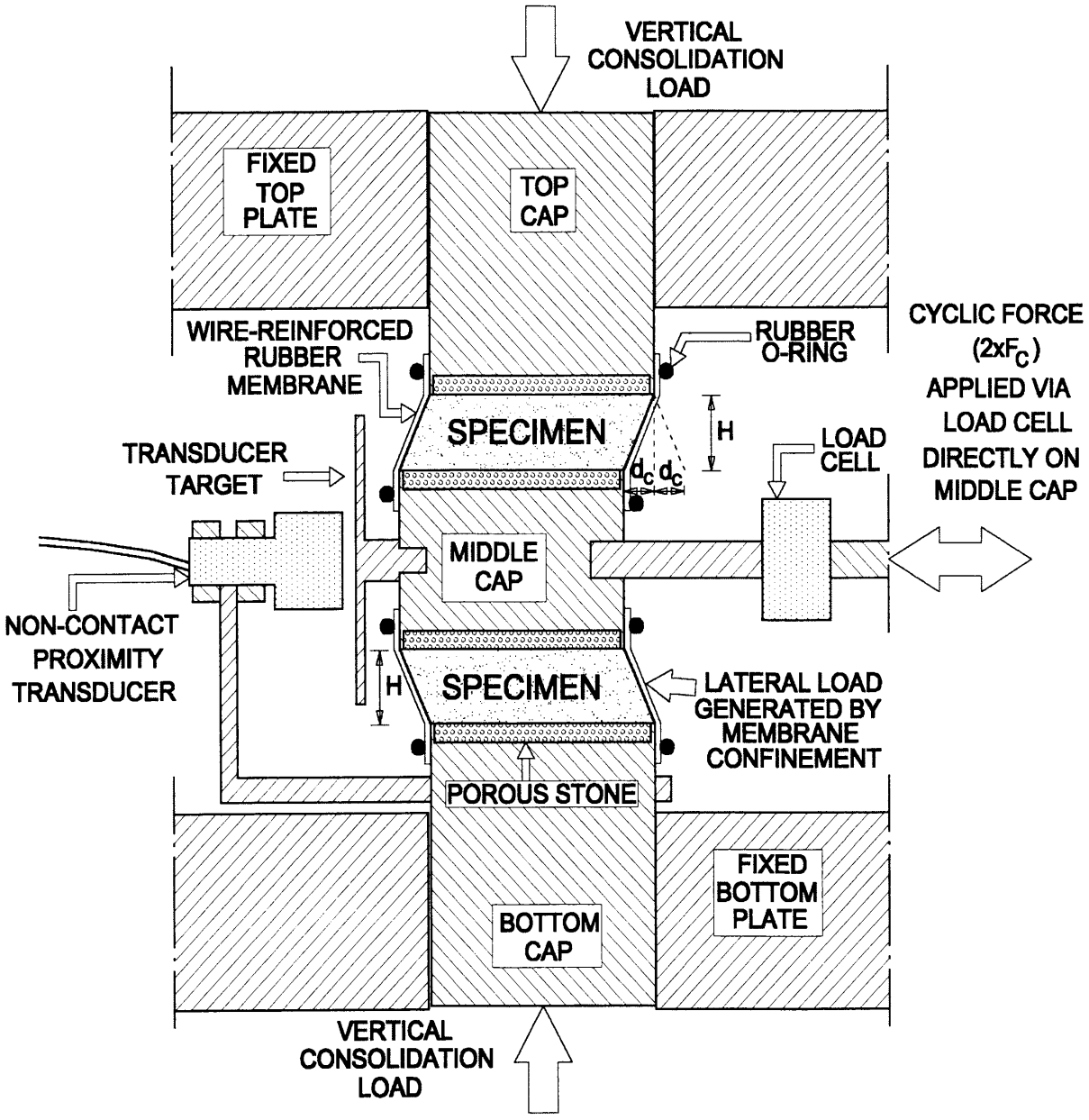

d_C = horizontal cyclic displacement amplitude
F_C = horizontal cyclic shear force
H = height of specimen
A = area of specimen
$\gamma_C = d_C / H$ = horizontal cyclic shear strain amplitude
$\tau_C = F_C / A$ = horizontal cyclic shear stress amplitude

Figure 4.1 Schematic of the UCLA Double Simple-Shear system.

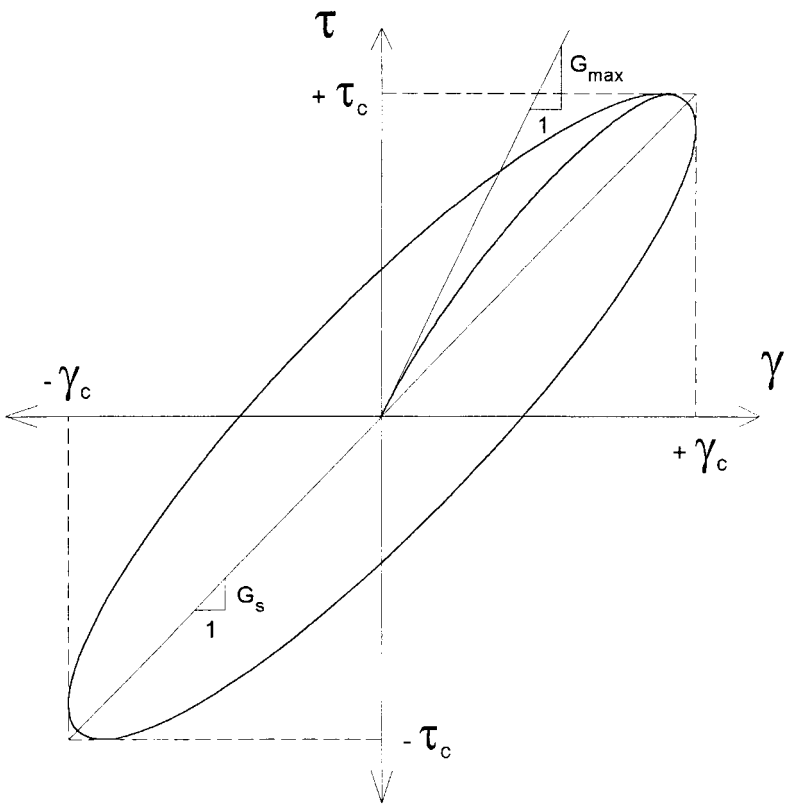

Figure 4.2 Idealized stress-strain loop during cyclic shearing, with parameter definition.

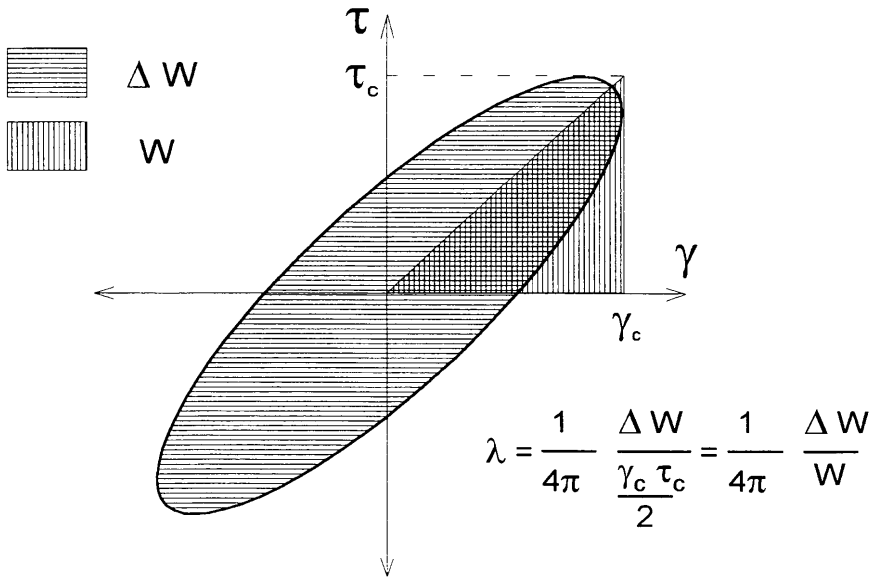

Figure 4.3 Definition of the equivalent viscous damping ratio used in this study.

Seven samples, recovered from depths between 12.1 and 37.2 m, were tested in a cyclic strain-controlled mode. The cyclic frequency was lower than 0.25 Hz. The dynamic properties of cohesionless soils are practically independent of loading frequency (Hardin, 1965), and tests on cohesive soils have shown the effect of frequency to be small so that it can be negligible (Kramer et al, 1992).

The test results are summarized in Figure 4.4. The variation of shear modulus with shear strain was measured over a broad range of strains. Values of the equivalent viscous damping ratio were also obtained for strains up to a least 10^{-4}.

The maximum shear modulus measured in the laboratory can be compared to that obtained from in-situ shear-wave velocity logs (Gmax). At UCR's Rivera site, for the seven locations where this comparison can be performed, between depths of 2.1 and 37.2 m, the ratio of laboratory to field values is between 0.13 and 0.54 (Table 4.3). This shows that, even with very careful sampling and handling techniques, there can be significant differences between the field and laboratory Gmax values, created by the transfer from the ground to the laboratory testing system.

For nonlinear soil dynamics computations, the laboratory moduli at the lowest strain (10^{-6}) are set to the value of Gmax, and the rest of the shear-strain shear-modulus curve is normalized to this Gmax value. This is based on the premise that the field values are representative of the properties of the undisturbed material. This procedure, commonly used in geotechnical engineering, has recently been compared by others investigators to several possible laboratory-to-field adjustments and was recommended as the best (Pitilakis and Anastasiadis, 1998).

Table 4.3: Ratio of laboratory Gmax to field Gmax for UCR soils

Depth (m)	Laboratory Gmax (MPa)	Field Gmax (Mpa)	Ratio, Laboratory/Field
2.1	30	55	0.54
3.7	48	265	0.18
9.5	46	355	0.13
18.1	93	405	0.23
24.4	150	545	0.28
32.3	220	754	0.29
37.2	116	619	0.19

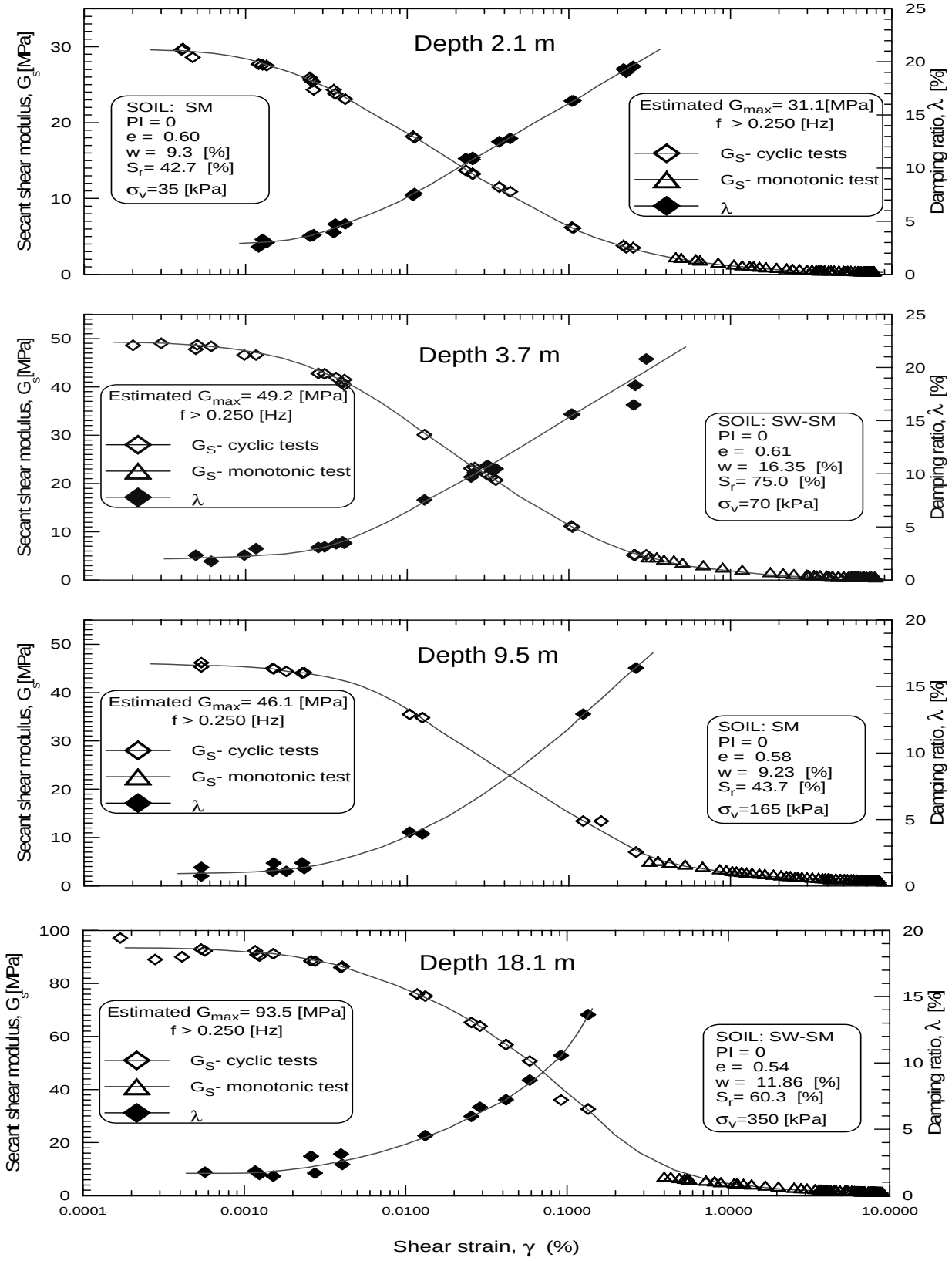

Figure 4.4 Summary of Simple Shear Test Results on Soils from the Rivera Library Site

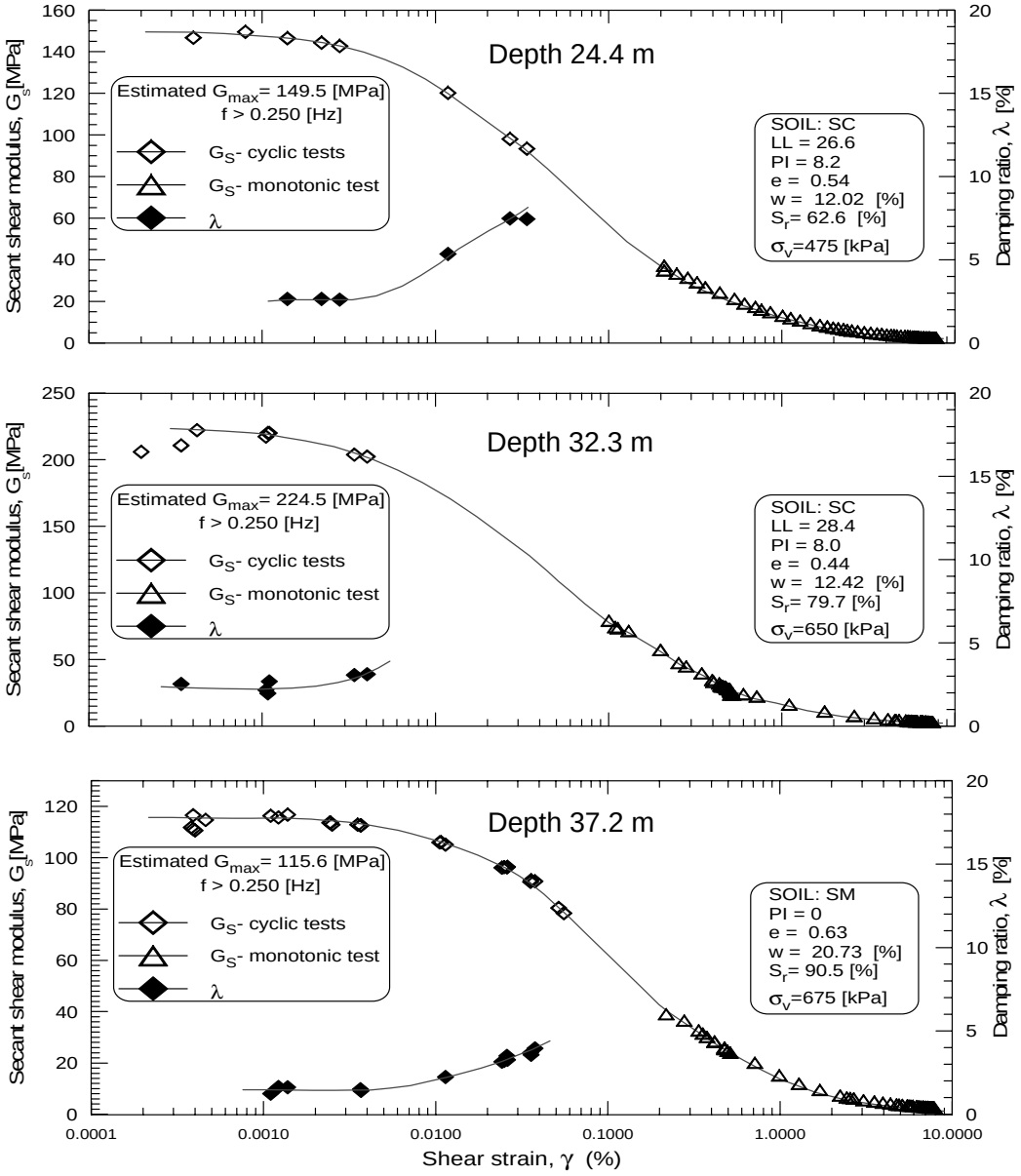

Figure 4.4 (cont.)

4.1.3 Monotonic Triaxial Tests

These tests were conducted in the Geotechnical Laboratory of the Department of Civil Engineering at U.C. Berkeley. The samples were first saturated, and then consolidated to a horizontal-to-vertical stress ratio of K = 0.6 prior to testing. All the tests were performed in drained conditions, using a strain-control mode. The U.C. Berkeley triaxial testing system is shown in Figure 4. The failure envelope for the UCR samples was very consistent for all but the deepest sample (37 m) at various degrees of lateral confinement (Figure 4.6). The effective cohesion is estimated at 40 kPA and the effective friction angle at 36 degrees.

Figure 4.5 The U.C. Berkeley triaxial testing System

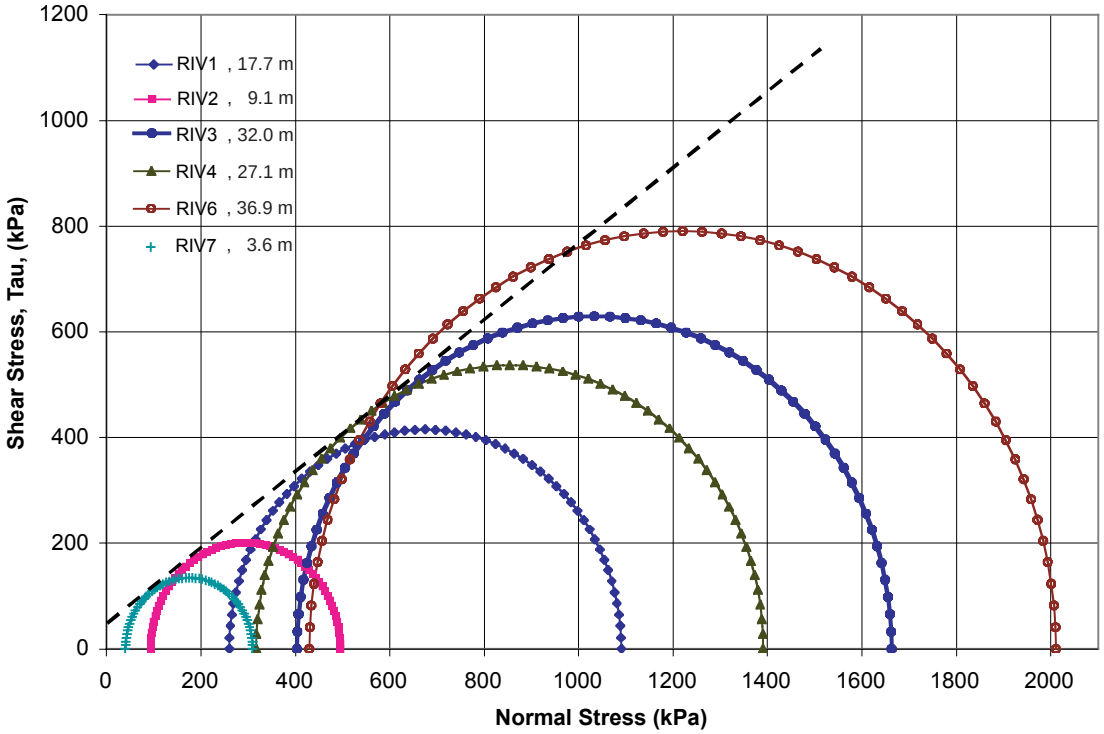

Figure 4.6 Drained triaxial test failure envelopes for the UCR Rivera soils.

4.2 Soil Dynamics Computational Models

4.2.1 The NOAH Soil Dynamics Computer Model

The computational model of nonlinear soil response to earthquake used for the CEP studies at UCR is a formulation from UCSB, by Bonilla et al., 1998. This NOAH (NOnlinear Analysis Hysteretic) model includes anelastic and hysteretic behavior, and is based on the assumption of one-dimensional vertical propagation of the three components (2 horizontal, 1 vertical) of earthquake motion. This is a common and reasonable assumption when there is no indication of potential effects due to basin or other geologic structure. The soil profile is represented as a series of horizontal layers. The model assumes continuum mechanics, and implements a finite-difference based numerical integration of the 1-D shear wave equation of motion with appropriate boundary and initial conditions:

$$\rho \frac{\partial^2 u}{\partial t^2} = \frac{\partial \tau}{\partial z} \tag{3.1}$$

Here $u(z,t)$ denotes the displacement field perpendicular to the vertical axis at position z and time t; ρ is the unstrained density of the material, and $\tau(z,t)$ is the shear stress.

The stress-strain relationship of the soil is described by a hyperbolic model, given by the following equation (Kondner and Zelasko, 1963):

$$\tau = \frac{G_{\max}\gamma}{1+\left|\frac{G_{\max}}{\tau_{\max}}\gamma\right|} + \eta\frac{\partial \gamma}{\partial t} \tag{3.2}$$

where $\gamma(z,t) = \partial u(z,t)/\partial z$ denotes the shear strain, $G_{\max}$ is the maximum shear modulus at low strain; $\tau_{\max}$ is the maximum stress that the material can support in the initial state, and η is the viscosity factor. The first term on the right hand side of eq. 3.2 corresponds to the anelastic properties, while the second term corresponds to energy dissipation by viscosity. The parameter $\eta = C_1 G_{\max}/C_2\pi$, with $0.01\% \le C_1 \le 1.0\%$ and $1.0 \le C_2 \le 5.0$ Hz. Equations (3.1) and (3.2) hold for both horizontal components of the shear stress. For the vertical stress and the vertical component of the displacement field $w(z,t)$, two similar relationships are used with u replaced by w and the parameter $G_{\max}$ replaced by M in the previous equations. The parameter $M = \rho v_p^2$ is the constrained modulus and v_p is the p-wave velocity (see Chen and Saleeb, 1982). In this representation, the values of the other parameters are assumed to be the identical for the three components in a given layer.

Hysteresis models have been discussed extensively in the literature (Pyke, 1979; Vucetic, 1990; McCall, 1994; Muravskii and Frydman, 1998; Yoshida et al., 1998, Xu et al., 1998, etc…). In

NOAH, for each of the three components, the hysteretic behavior is implemented with the generalized Masing rules (Archuleta et al., 1999, 2000a). This new formulation of hysteresis is based on the original Masing rules (Masing, 1926, Kramer, 1996). The generalized Masing rules provide a framework for understanding the non-uniform dilation and translation of stress-strain loops for a material subject to non-periodic stresses (or strains). This new hysteresis formulation has several interesting features. It has a functional representation and it includes the Cundall-Pyke hypothesis (Pyke, 1979) and Masing's original formulation as special cases. In its most elementary implementation, the generalized Masing rule is even simpler than the Masing and extended Masing rules (Kramer, 1996). The model depends only on one free parameter γ_f named the fiducial point. This parameter controls the size of the loop in the stress-strain space and therefore can be related to the amount of energy dissipated through the nonlinear property of the material. In other words, the generalized Masing rules provide a mean to introduce the effect of the damping ratio into nonlinear modeling independently of the other soil parameters (Ishihara, 1996). The relationship between the anelastic damping of a stress-strain loop and the fiducial point for cyclic loadings has been derived in Archuleta et al., 1999.

In the Generalized Masing rules, the initial loading is given by the backbone curve $F_{bb}(\gamma)$ (eq. 3.2). For the subsequent loadings and unloadings, the strain-stress relationship is given by the following tranformation:

$$\frac{\tau - \tau^{(i)}}{c_H} = F_{bb}\left(\frac{\gamma - \gamma^{(i)}}{c_H}\right) \tag{3.3}$$

until the path prescribed by eq. (3.3) crossed the backbone curve (eq. 3.2) in the stress-strain space (Figure 3.9). Then the current loading or unloadings return to the backbone curve until the next turning point where eq (3.3) is applied again and the rules are iterated. The coordinate $(\gamma^{(i)},\tau^{(i)})$ corresponds to the i^{th} (and previous) reversal points in the strain-stress space (see Figure 3.9 for an illustration with $i=1$ and 2). In Masing's original formulation, the hysteresis scale factor c_H is equal to 2.0. In the generalized Masing rules, c_H is a function of physical properties of the material and of γ_f (Archuleta et al., 1999, 2000a). In the stress-strain space, γ_f controls the intersection between the path given by eq. (3.3) and the backbone curve.

The Generalized Masing rules can be summarized by the following relation:

$$\tau(\gamma) = \begin{cases} F_{bb}(\gamma) & \gamma < \gamma^{(1)}, t < t^{(1)} \\ c_H^{(n)} F_{bb}\left(\dfrac{\gamma - \gamma^{(n)}}{c_H^{(n)}}\right) + \tau^{(n)} & |\gamma| \le |\gamma_f|, t \ge t^{(1)} \\ F_{bb}(Sign\left(\frac{d\gamma}{dt}\right)\gamma) & |\gamma| \ge |\gamma_f|, t \ge t^{(1)} \end{cases} \tag{3.4}$$

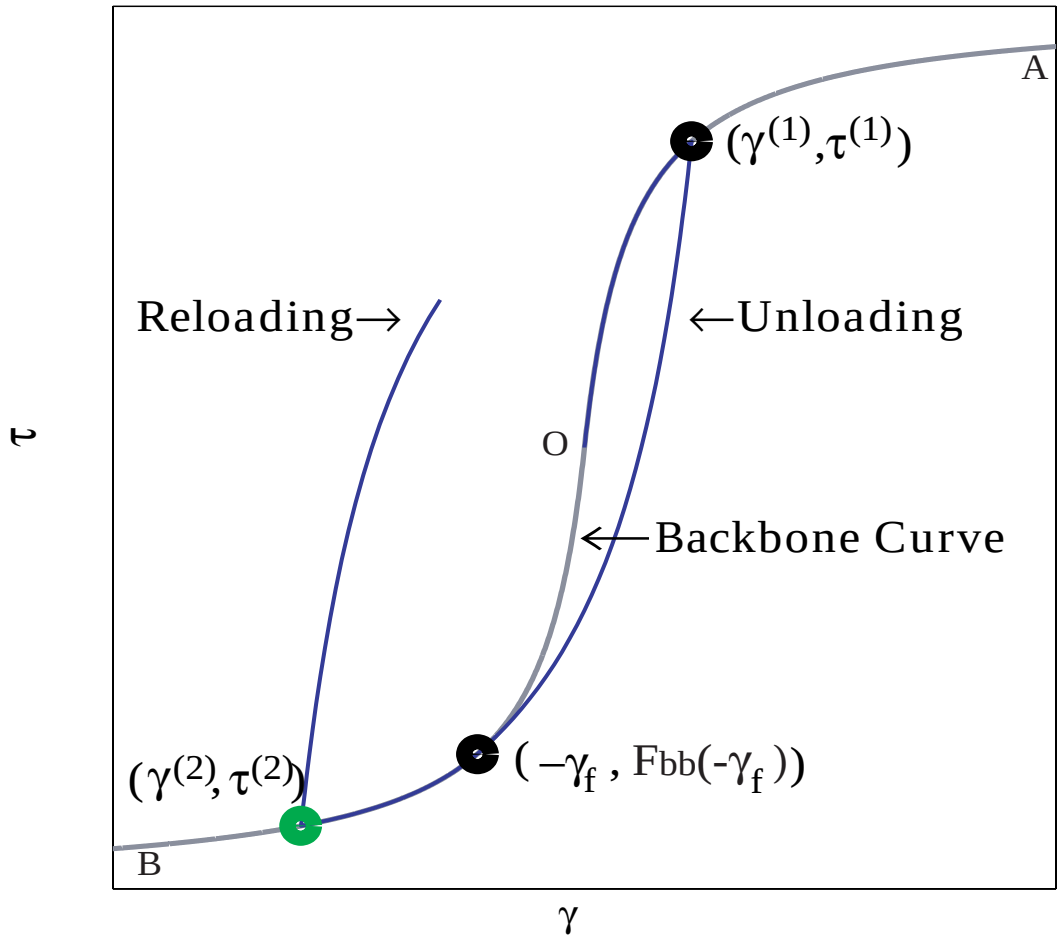

Figure 4.7 Path followed by the stress-strain curve for a soil under noncyclic loading with hysteretic properties controlled by the generalized Masing rules (NOAH model).

where $t^{(1)}$ is the time corresponding to the first turning point and $\tau^{(n)}$ is given by the following relation:

$$\tau^{(n)} = \sum_{i=2}^{n} c_H^{(i-1)} F_{bb}\left(\frac{\gamma^{(i)} - \gamma^{(i-1)}}{c_H^{(i-1)}}\right) + F_{bb}\left(\gamma^{(1)}\right) \qquad (3.5)$$

where $\gamma^{(n)}$ corresponds to the turning point at the n^{th} unloading or reloading (the index n is even at reloading and odd when unloading). The time derivative in eq. (3.4) is estimated at any time between the n^{th} and the $(n+1)^{th}$ turning point. The function *Sign* is 1 when its argument is positive, 0 when the argument is 0, and -1 when its argument is negative. The third rule in eq. (3.4)

does not apply for $\gamma_f \to \infty$ and is optional for $\gamma_f = \gamma^{(1)}$. With reference to Figure 3.9, the first rule in the right hand side of eq. (3.5) corresponds to the first loading path. The second rule governs the hysteresis behavior of successive unloading and reloading paths until $|\gamma|$ exceeds $|\gamma_f|$. Note that for an aperiodic signal, successive unloading and reloading paths can occur with the strain stress path not necessarily crossing the backbone curve. Although each unloading path, or reloading path, follows a track in the stress-strain space directed to the fiducial point $[(-\gamma_f, F_{bb}(-\gamma_f)]$, or $[\gamma_f, F_{bb}(\gamma_f)]$, it may not reach this point if a reversal takes place before getting to the fiducial point. (Each of these reloading/unloading paths are characterized by turning points $|\gamma^{(n)}| < |\gamma_f|$ with $n > 1$.) The term $\tau^{(n)}$, given by eq. (3.5), is determined by the contribution of the previous turning point. When $|\gamma| > |\gamma_f|$, the third rule in eq. (3.4) specifies that the stress-strain path follows the backbone equation. Memory of all previous turning points is erased each time the strain-stress path returns to the backbone curve.

When the backbone curve is given by the hyperbolic model (eq. 3.2), the expression for $c_H^{(n)}$ is given by the following relation:

$$c_H^{(n)} = \frac{\left(F_{bb}(Sign\left(\frac{d\gamma}{dt}\right)|\gamma_f|) - \tau^{(n)}\right)\left|Sign\left(\frac{d\gamma}{dt}\right)|\gamma_f| - \gamma^{(n)}\right|}{\left(Sign\left(\frac{d\gamma}{dt}\right)|\gamma_f| - \gamma^{(n)}\right)\tau_{\max} + \left(\tau^{(n)} - F_{bb}(Sign\left(\frac{d\gamma}{dt}\right)|\gamma_f|)\right)\gamma_{ref}} \qquad (3.6)$$

where the reference strain $\gamma_{ref} = \tau_{\max}/G_{\max}$. Note that, in general, the parameter $c_H^{(n)}$ will have a different value for different unloadings or reloadings. It is convenient to bound the parameter γ_f by the following relationship $|\gamma^{(1)}| \le |\gamma_f| < \infty$, where $\gamma^{(1)}$ corresponds to the first turning point and the upper bound corresponds to the Cundall-Pyke hypothesis (Pyke, 1979). For the CEP ground motion calculations $\gamma_f = \gamma^{(1)}$ with implementation of the third rule in eq. (3.4).

The NOAH code provides both total stress and effective stress formulations. Because of the great depth of the water table at U.C. Riverside, the total stress formulation was used in the calculations of surface strong motions.

4.2.2 Comparison of NOAH with Other Nonlinear Soil Models

The field of nonlinear dynamic analysis is much more complex than that of linear analysis. It behooves calculators to make every effort to verify their nonlinear calculations. Since analytical, exact solutions are very scarce for such purpose, an accepted practice is to compare the results

obtained with different nonlinear models. In order to assess the calculations performed with the NOAH model, the CE P also took advantage of the availability of other soil dynamics models in the U.C. community. Two additional such codes were exercised. Both perform three-component one–dimensional wave propagation through nonlinear soils. The first one is the SUMDES (Sites Under Multi-Directional Earthquake Shaking) code from U.C. Davis ((Li et al, 1992). Its formulation is based on "bounded surface" plasticity, and it can do effective stress analysis. The second one is the CYCLIC code from U.C. San Diego (Elgamal, 1991, 1999a, 1999b). It is an effective stress formulation, as well. Additional information regarding CYCLIC is available on line at http://casagrande.ucsd.edu. The excellent agreement between the calculations with the three different models is described in detail in the Phase 2 report for U.C. Santa Barbara (Archuleta et al., 2000b) and will not be repeated in full here. An example of the comparison is given in Figure 4.8.

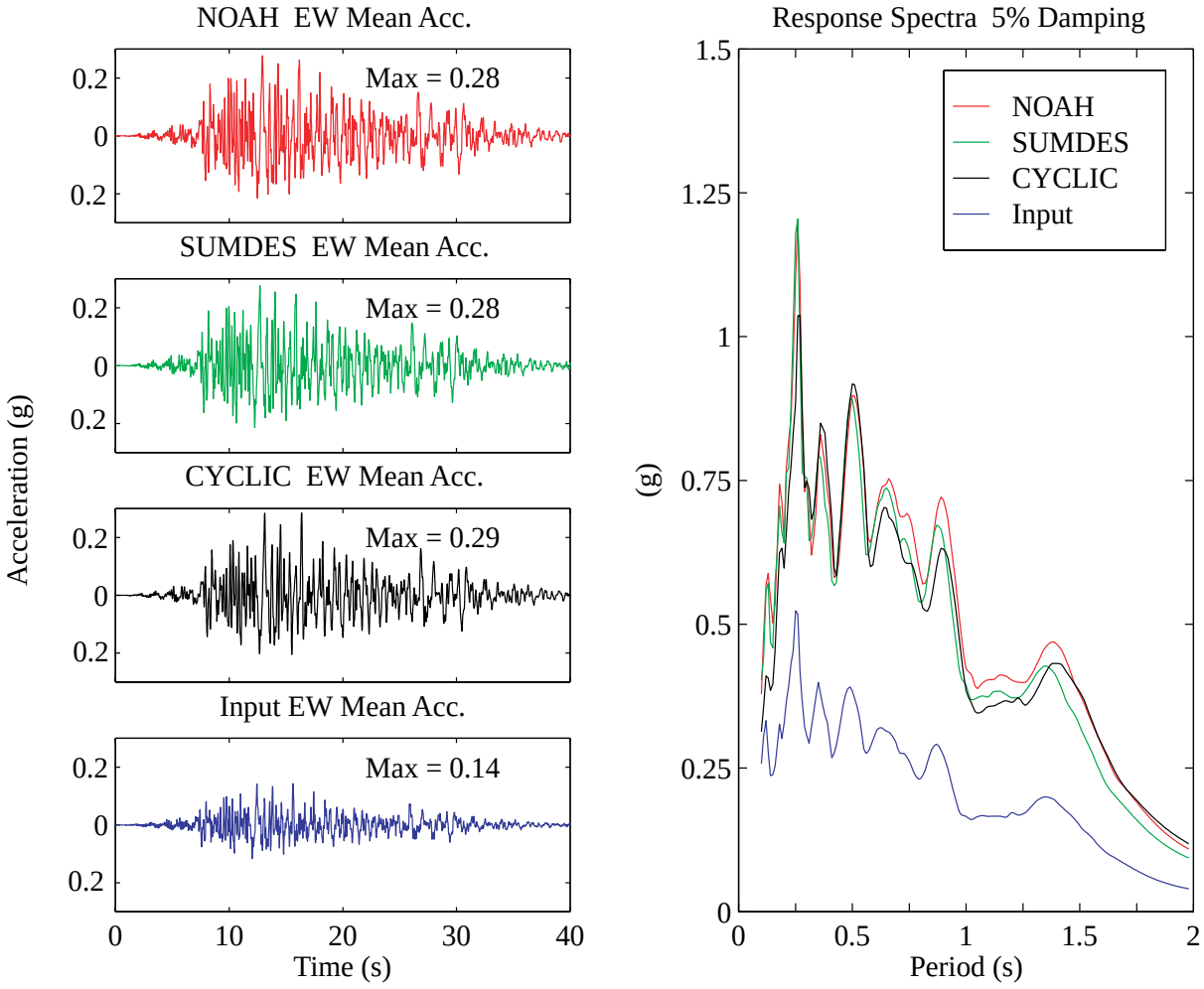

Figure 4.8 Comparison of NOAH, SUMDES, and CYCLIC results for a strong motion study of U.C. Santa Barbara (after Archuleta et al., 2000b).

4.2.3 UCR Soil Profiles and their Validation

The soil profiles for the three UCR sites were derived primarily from the suspension velocity logs, with additional input from the gamma and resistivity logs. The layers and the soil properties defined for the soil dynamics calculations are summarized in Tables 4.4 to 4.6.. The quality factor Q is $Q=1/2\lambda$ where λ is the damping ratio (percentage) at low strain. For all layers, the coefficient of earth pressure at rest is $K_0=0.5$, and the angle of internal friction $\phi=36°$.

Table 4.4. Computational soil profile at the Rivera library. The water table is located at 71-m depth.

Layer No.	Depth (m)	Vs (m/s)	Vp (m/s)	Unit weight (kg/m^3)	Q
1	3.0	212	354	1866	16.66
2	8.0	386	655	2028	50.00
3	10.0	352	678	1906	25.00
4	19.0	419	761	1996	25.00
5	21.0	570	973	2190	20.00
6	27.0	557	1026	2039	25.00
7	29.5	818	1391	2250	25.00
8	35.5	757	1340	2192	25.00
9	38.0	647	1191	2028	33.33
10	40.0	769	1328	2192	33.33
11	42.0	862	1583	2250	33.33
12	46.0	696	1292	2035	33.33
13	47.5	872	1557	2250	33.33
14	49.5	651	1256	2030	33.33
15	54.5	781	1441	2195	33.33
16	58.5	837	1528	2250	33.33
17	63.0	718	1317	2195	33.33
18	71.0	819	1542	2250	33.33
19	74.0	780	2132	2195	33.33
20	76.5	904	2205	2270	33.33
21	86.0	972	2422	2275	33.33
22	87.5	1118	2698	2300	33.33
23	89.0	1429	3229	2300	33.33

Table 4.5 Computational soil profile at Parking Lot 13. The water table is at 59.5-m depth

Layer No.	Depth (m)	Vs (m/s)	Vp (m/s)	Unit weight (kg/m^3)	Q
1	4.0	184	408	1866	16.66
2	12.0	252	493	1906	25.00
3	16.0	367	703	1906	25.00
4	23.0	550	1017	2190	20.00
5	59.5	813	1426	2250	33.33
6	66.0	775	2168	2195	33.33
7	69.0	1200	2946	2195	33.33

Table 4.6 Computational soil profile at Parking Lot 16. The water table is at 71-m depth

Layer No.	Depth (m)	Vs (m/s)	Vp (m/s)	Unit weight (kg/m^3)	Q
1	3.0	264	507	1866	16.66
2	8.0	256	456	2028	50.00
3	10.0	275	503	1906	25.00
4	16.0	378	706	1996	25.00
5	21.0	439	838	2190	20.00
6	27.0	456	897	2038	25.00
7	29.5	571	1214	2250	25.00
8	35.5	720	1268	2192	25.00
9	38.0	725	1291	2028	33.33
10	40.0	688	1262	2192	33.33
11	42.0	781	1450	2250	33.33
12	46.0	718	1265	2035	33.33
13	47.5	816	1431	2250	33.33
14	49.5	871	1559	2030	33.33
15	54.5	772	1468	2195	33.33
16	58.5	767	1420	2250	33.33
17	63.0	833	1538	2195	33.33
18	71.0	816	1597	2250	33.33
19	74.0	853	2274	2195	33.33
20	76.5	873	2330	2270	33.33
21	86.0	914	2347	2275	33.33
22	87.5	1 082	2542	2300	33.33
23	89.0	1066	2532	2300	33.33
24	93.5	1013	2474	2300	33.33
25	95.5	750	2150	2300	33.33
26	102.0	1013	2474	2300	33.33
27	104.0	1800	3700	2300	33.33

The extensive field and laboratory characterization of the UCR soils lends confidence in the numerical model of the UCR sites. Nevertheless, the availability of actual earthquake records at the surface and at depth below the Rivera site provides an opportunity for further checking of that model and, by extension, of the models for the other sites. To achieve this, downhole motions are calculated from surface records and compared to the recorded downhole motions. This is illustrated in Figure 4.9 using the March 22, 1999 M 3.8 event that was the EGF for the UCR syntheses. The comparison is satisfactory and shows that the 1-D wave propagation assumption is reasonable for the UCR sites. The difference between calculated and observed motions possibly is due to the sloping bedrock basement under UCR. Because the surface records will reflect these 3-D effects, those records are the right choice for synthesizing large motions, as was done on the CEP.

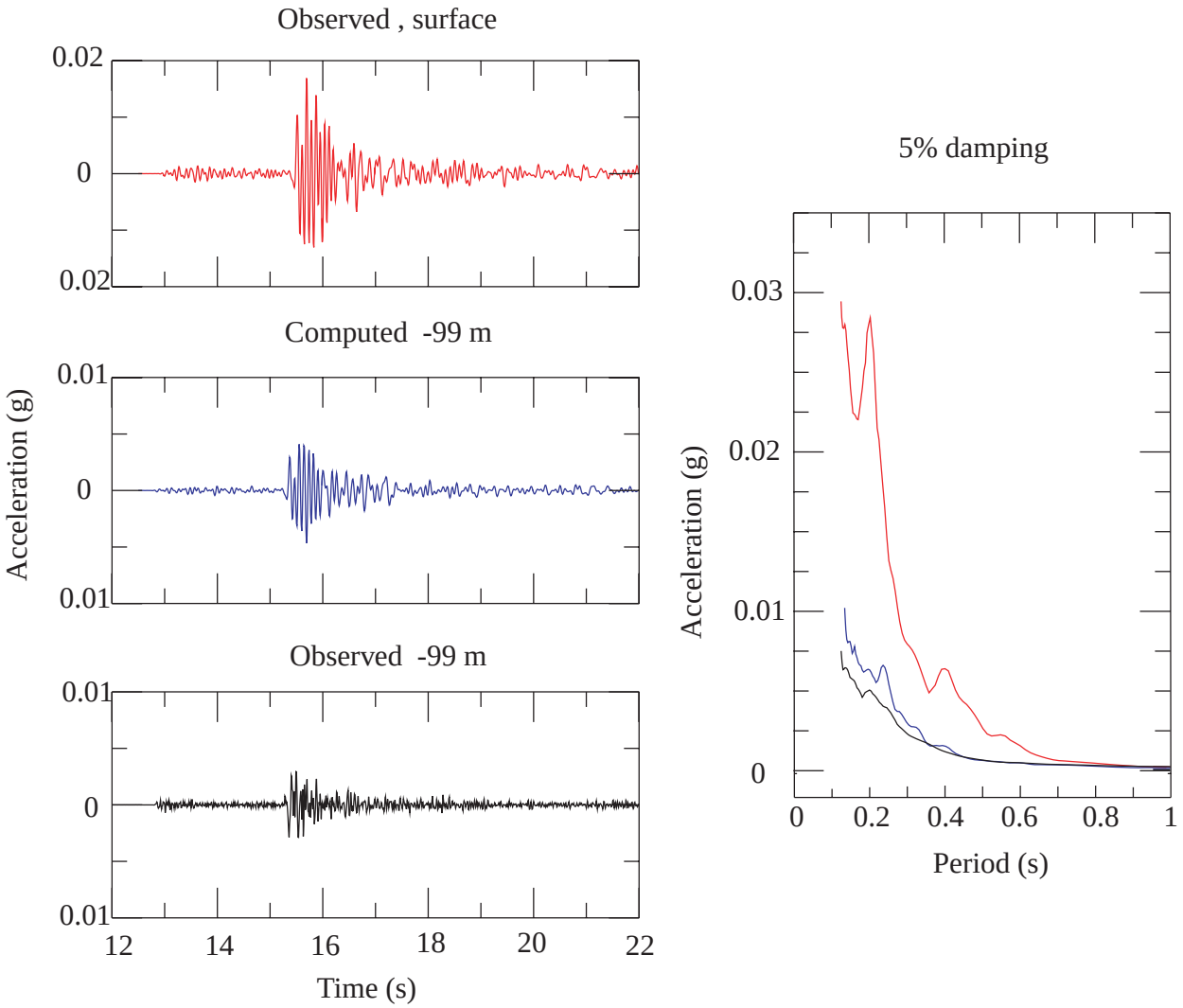

Figure 4.9 Calculated vs. recorded horizontal motions at - 99 m under the Rivera site, for the EW component of the March 22, 1999 earthquake which was used as the Empirical Green's function.

4.3 The CEP Surface Strong Motion Estimates

4.3.1 Calculations of Surface Strong Motions for UCR

The set of 120 time-histories of incident downhole motions were propagated to the surface of the three sites through the respective soil profiles with the NOAH model. The results are shown on Figures 4.10 to 4.12 in terms of spectral accelerations vs. period. The three spectral lines are respectively the mean and the plus and minus one standard deviation of the scenario population.

4.3.2 Comparison of Surface Motions at the Three UCR Sites

The mean and + 1 sigma horizontal surface acceleration spectra for the three UCR sites are compared in Figures 4.13 and 4.14. Representative time-histories in the EW and NS directions are compared in Figures 4.15 and 4.16. It can be seen that there are no major differences in the character of the motions. The responses at the 3 sites previously had been found to be comparable, in the analysis of small motion records from the surface deployment, performed by Lawrence (1999). These results are consistent with the fact that the soils under the three sites are of equivalent properties and the soil depth is in excess of 30 m. Accordingly, at UCR locations where the soils under UCR basically stay within the range of properties determined at the three sites studied in this phase of the CEP study, the estimated motions can be used as representative. At locations where the bedrock is shallower than 30 m less severe motions could be expected.

4.3.3 Comparison of Calculations with NOAH and the CYCLIC Model

An independent check of the NOAH results was performed by also calculating the surface motions using the CYCLIC model. A representative acceleration time-histories was selected, and propagated to the surface for the Rivera site. It is the EW component for a + 1 sigma scenario. The results are shown in terms of acceleration response spectra in Figures 4.17. The two nonlinear soil dynamics calculations gave very consistent results.

4.3.4 Nonlinear Behavior of UCR Soils

The CEP estimates of surface motions use nonlinear soil dynamics models because of the presumed nonlinear response of soils to the strong motions. This assumption is corroborated by the level of shear strains expected in a M 7.0 event on the San Jacinto fault. Figure 4.18 shows a profile of maximum shear strain in the UCR soil column, versus depth, for a mean and a mean + 1 sigma scenario in the NS direction at the Rivera site. Based on the modulus degradation curves of section 4.1.2 (Figure 4.4) the shear modulus of the soils in the top 30 m may be reduced by up to 80% in a mean scenario and 85% in a + 1 sigma scenario.

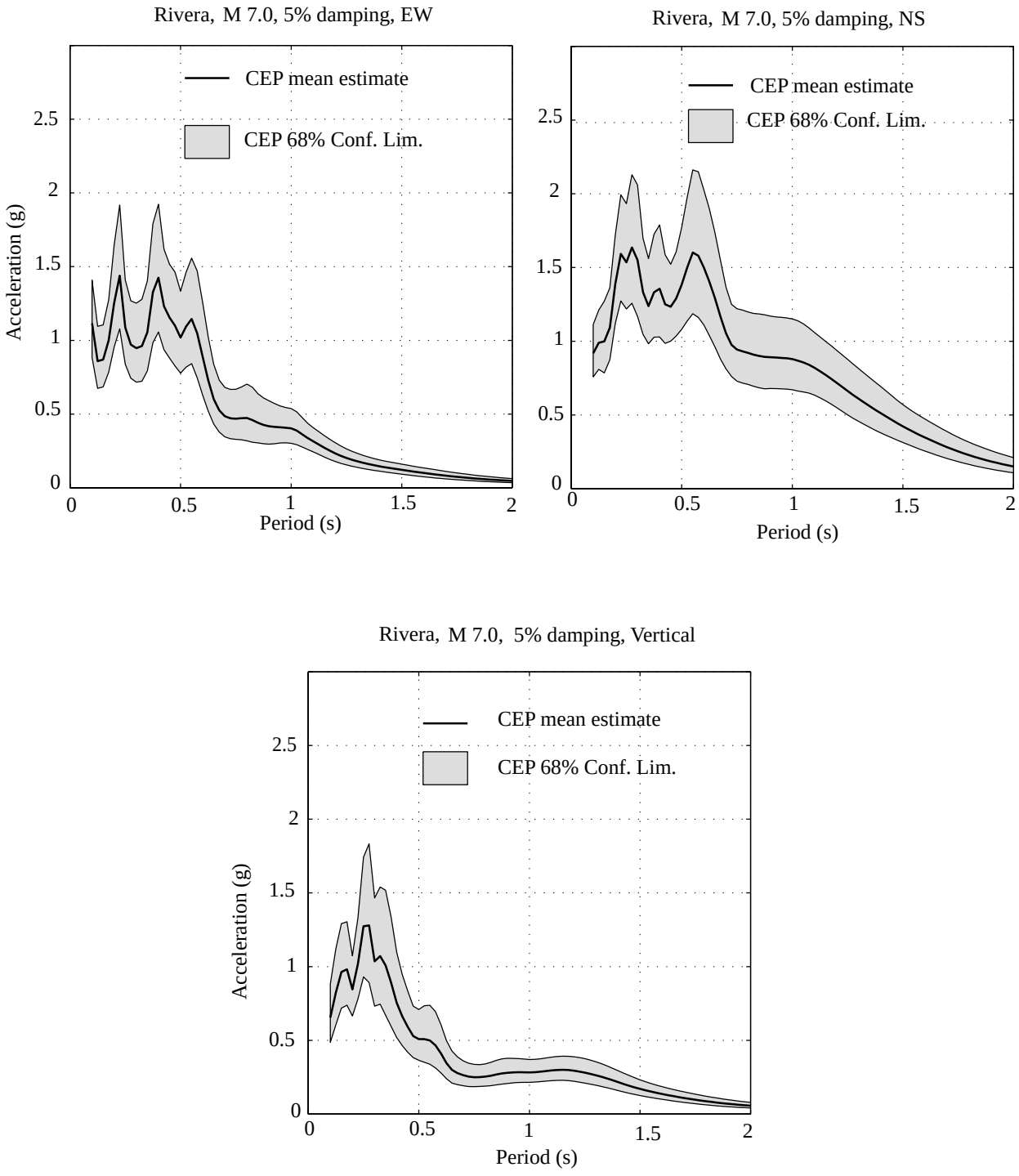

Figure 4.10 CEP surface acceleration response spectra at the Rivera library site.

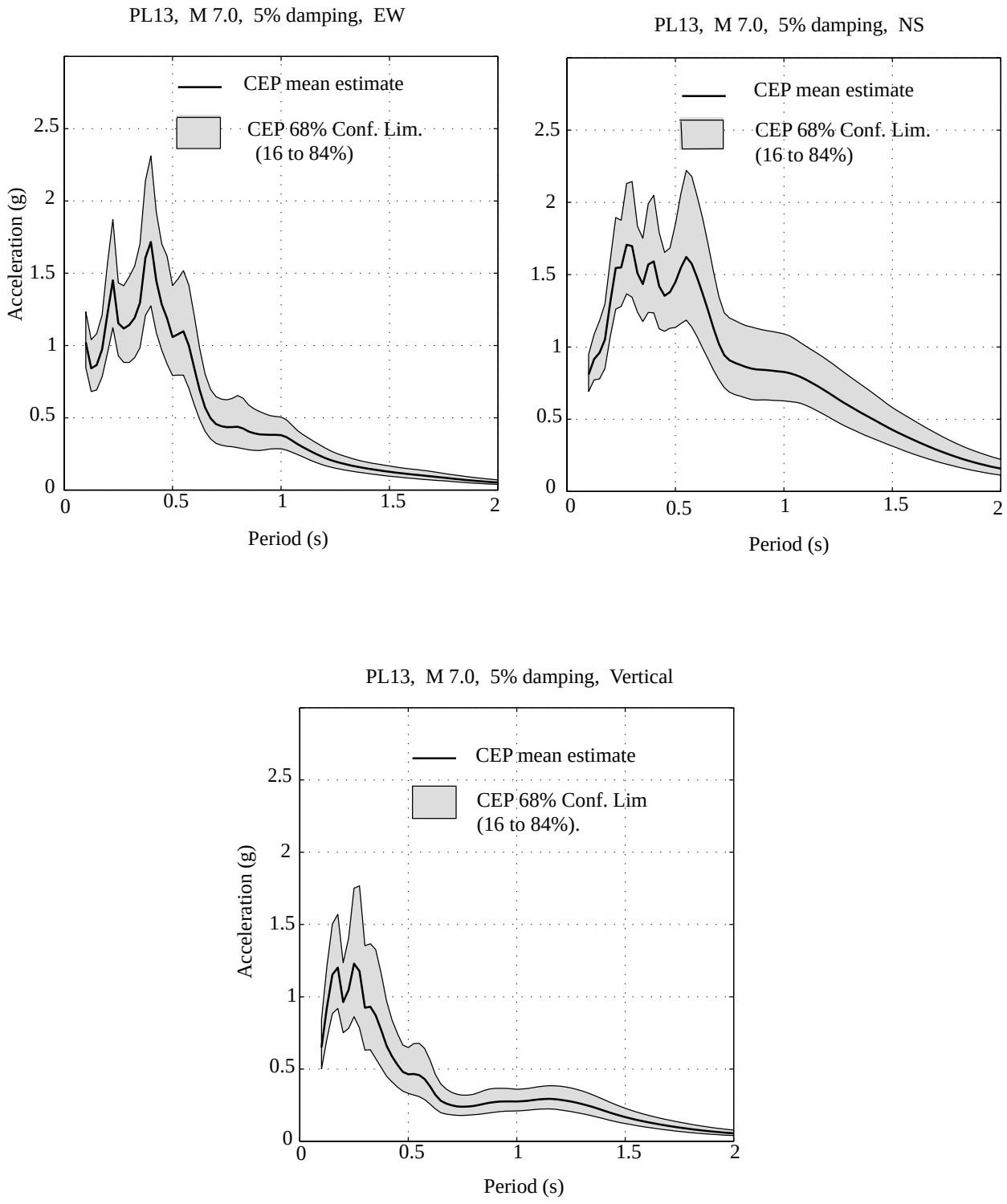

Figure 4.11 CEP surface acceleration response spectra at the Parking Lot 13 site.

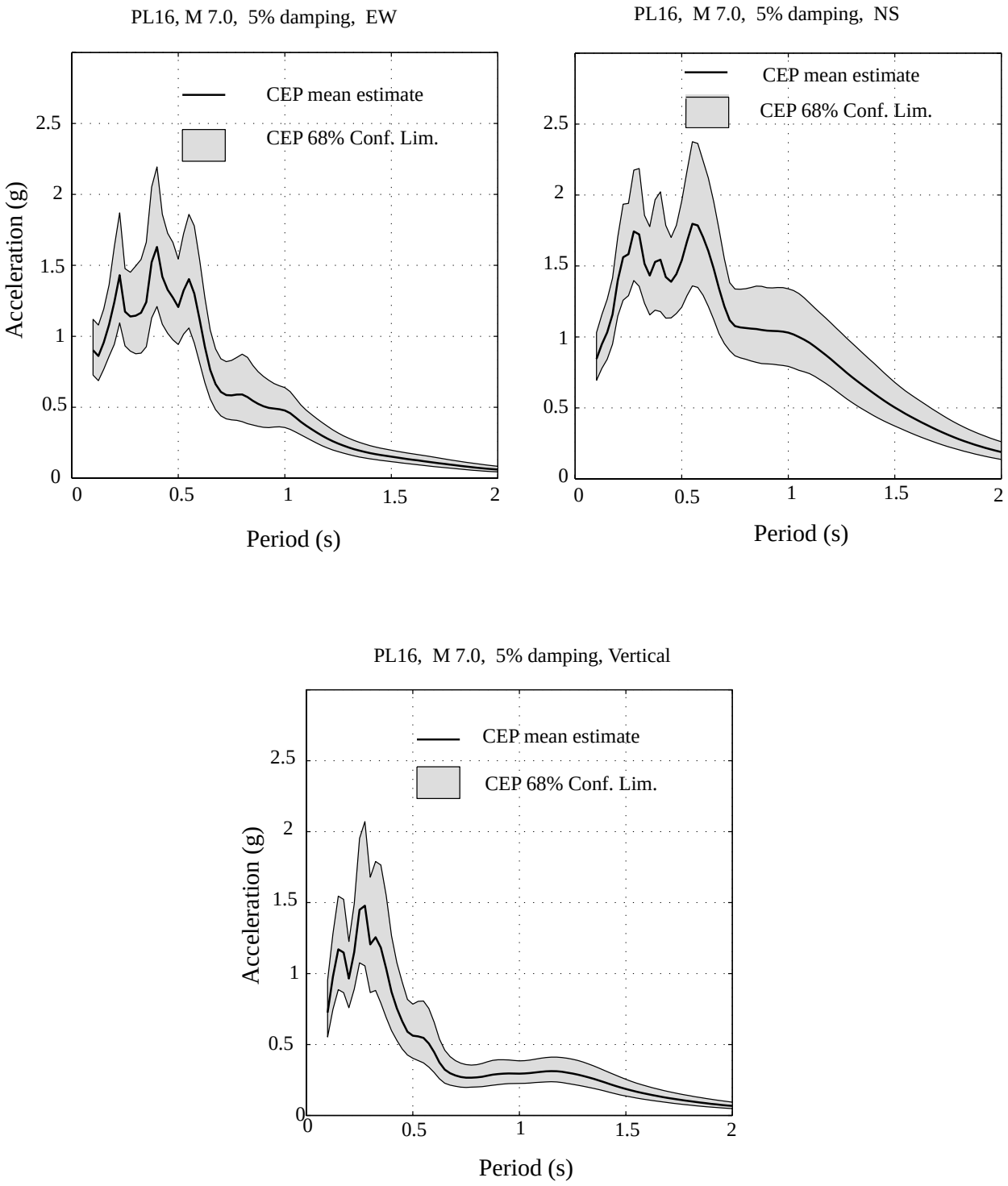

Figure 4.12 CEP surface acceleration spectra at the Parking Lot 16 site.

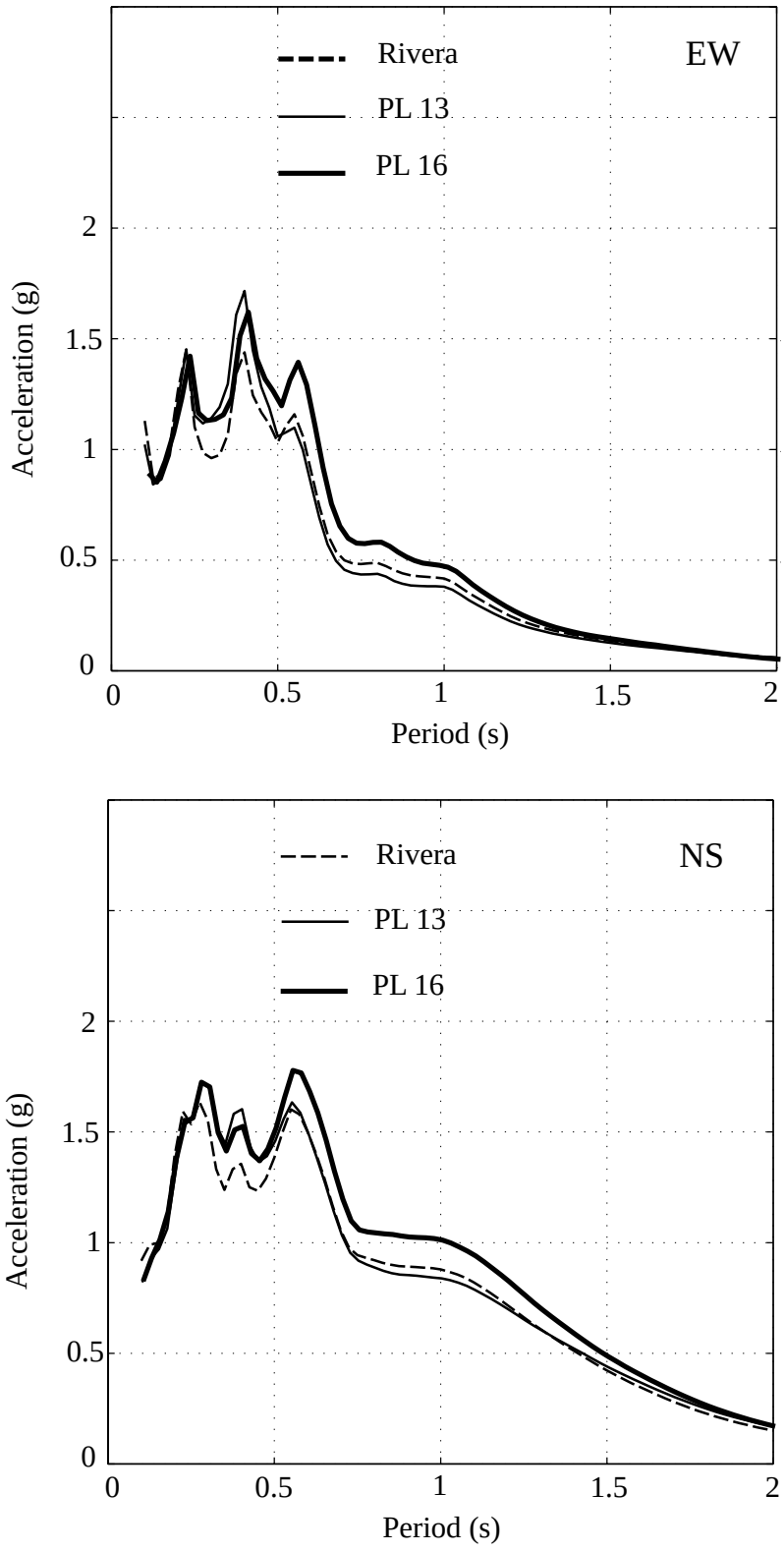

Figure 4.13 Comparison of mean horizontal acceleration response spectra for the 3 UCR sites

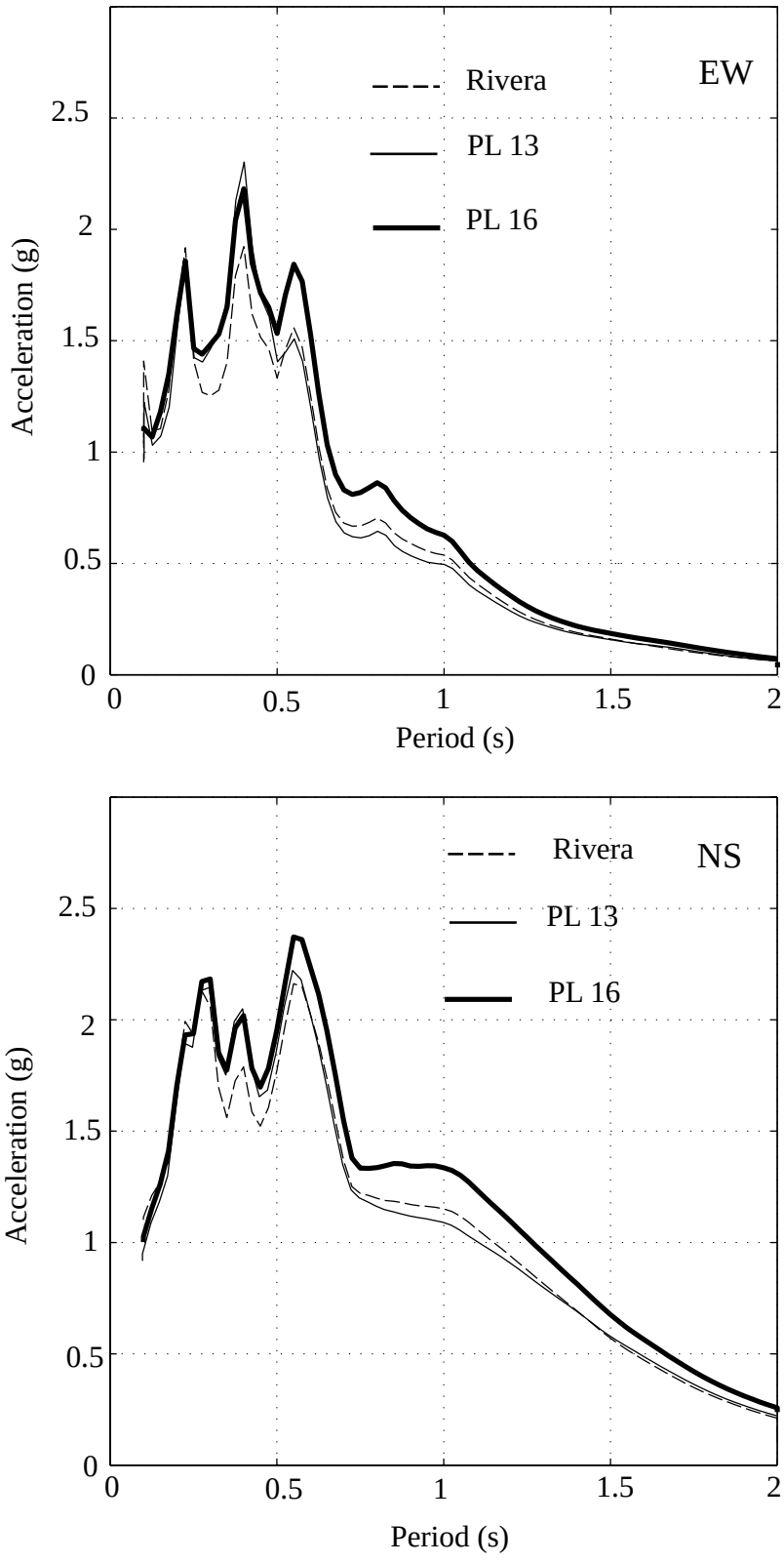

Figure 4.14 Comparison of + 1 sigma surface acceleration response spectra for the 3 UCR sites.

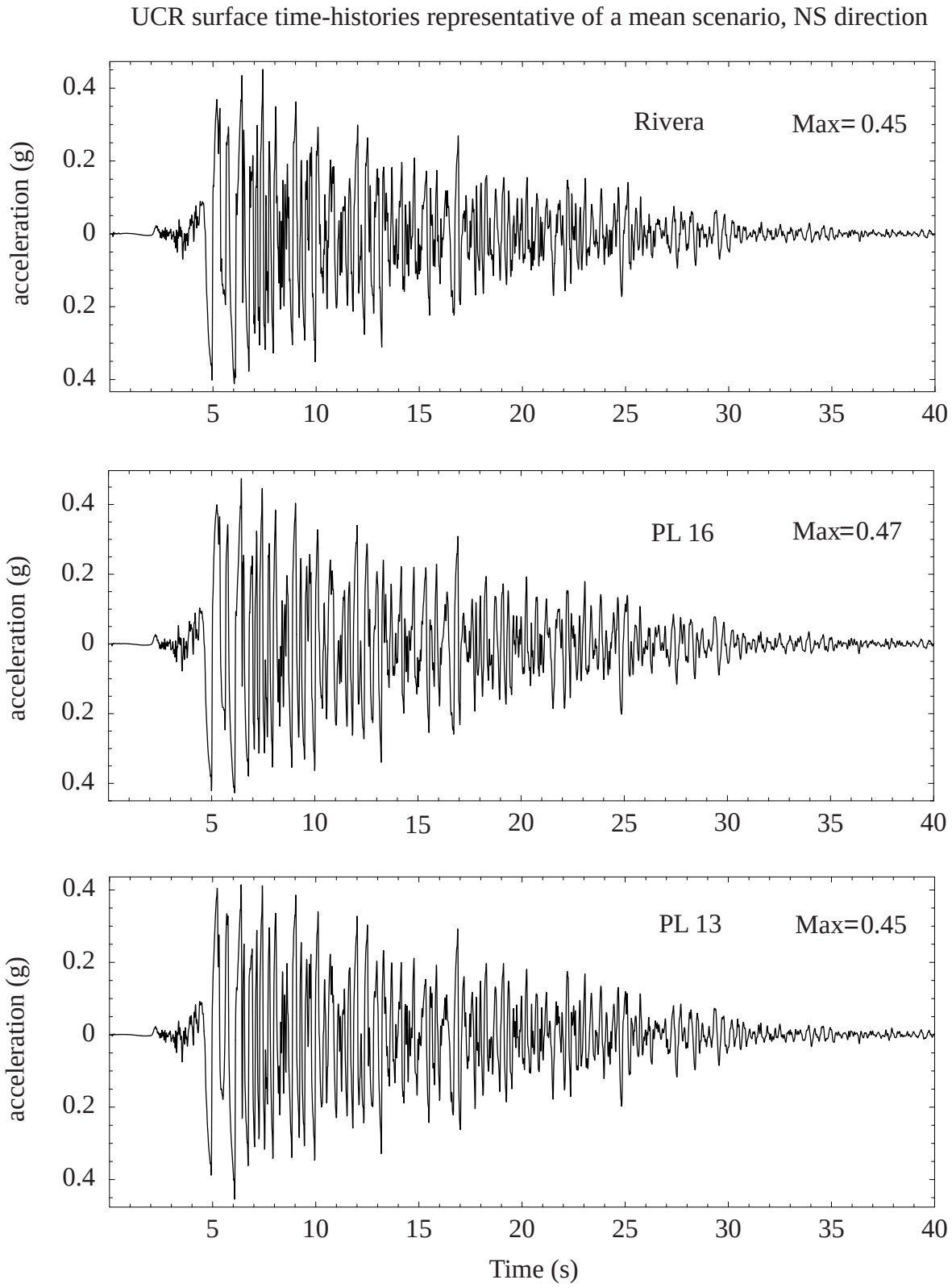

Figure 4.15 Comparison of mean scenario representative NS time-histories at the 3 UCR sites

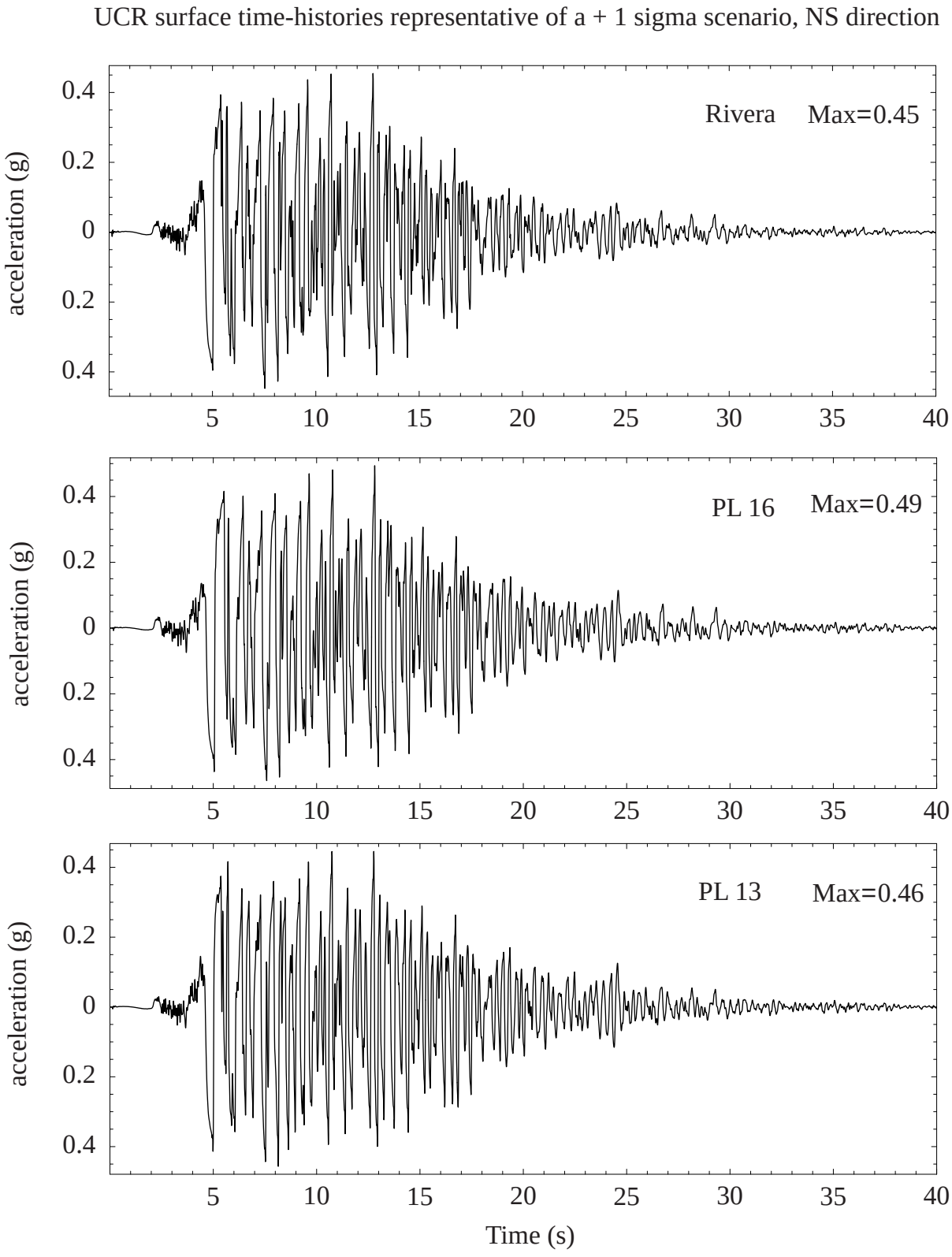

Figure 4.16 Comparison of + 1 sigma scenario representative NS time-histories at 3 UCR sites.

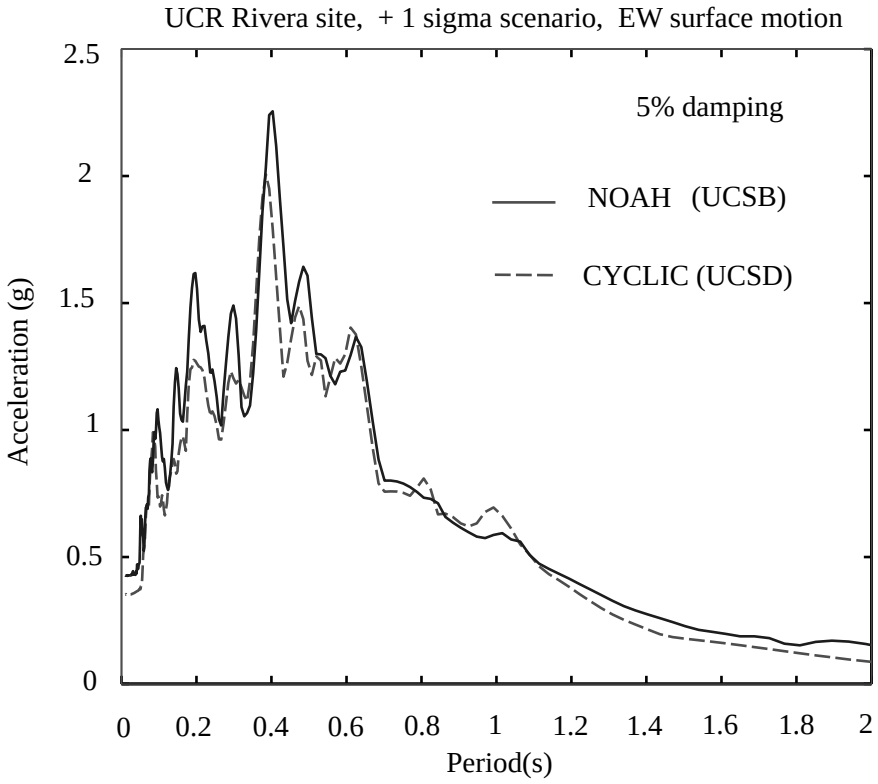

Figure 4.17 Comparison of surface motions calculated with the NOAH and CYCLIC models

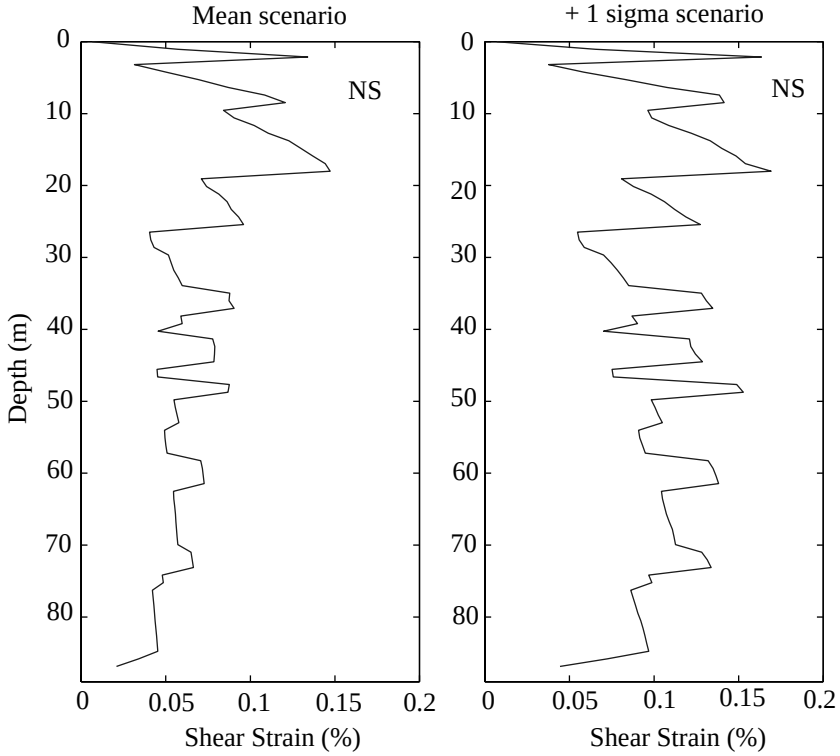

Figure 4.18 Maximum NS shear strains in the soil column of the Rivera site under a M 7.0 event.

4.4 Overall Comparison of the CEP and State-of-the-Practice Estimates

Typically, one would obtain ground motion estimates for the UCR site by using other approaches. One is the 1997 Uniform Building Code (UBC 97) procedure. The outcome is shown in Figure 4.19 for 5% damping and for a Soil C site condition, based on the results of the CEP geophysical logging, and on the relevant causative fault(s) (see International Conference of Building Officials/ICBO, 1998). We also show the General Procedure Response Spectrum based on the 2000 International Building Code (ICBO, 2000).

Another approach is to obtain estimates from Probabilistic Seismic Hazard Analyses (PSHA), such as those based on the research of the California Department of Mines and Geology (Petersen et al, 1996; Blake, 1999). The results are also shown on Figure 4. for recurrence probabilities of 10%, 5%, and 2% in 50 years (return periods of 475, 950, and 2375 years respectively). The Design-Basis Earthquake (DBE) used for the retrofit of the Rivera library building is also included in Figure 4. It is very clear that this DBE assumption is significantly lower than current state-of-the practice estimates would provide.

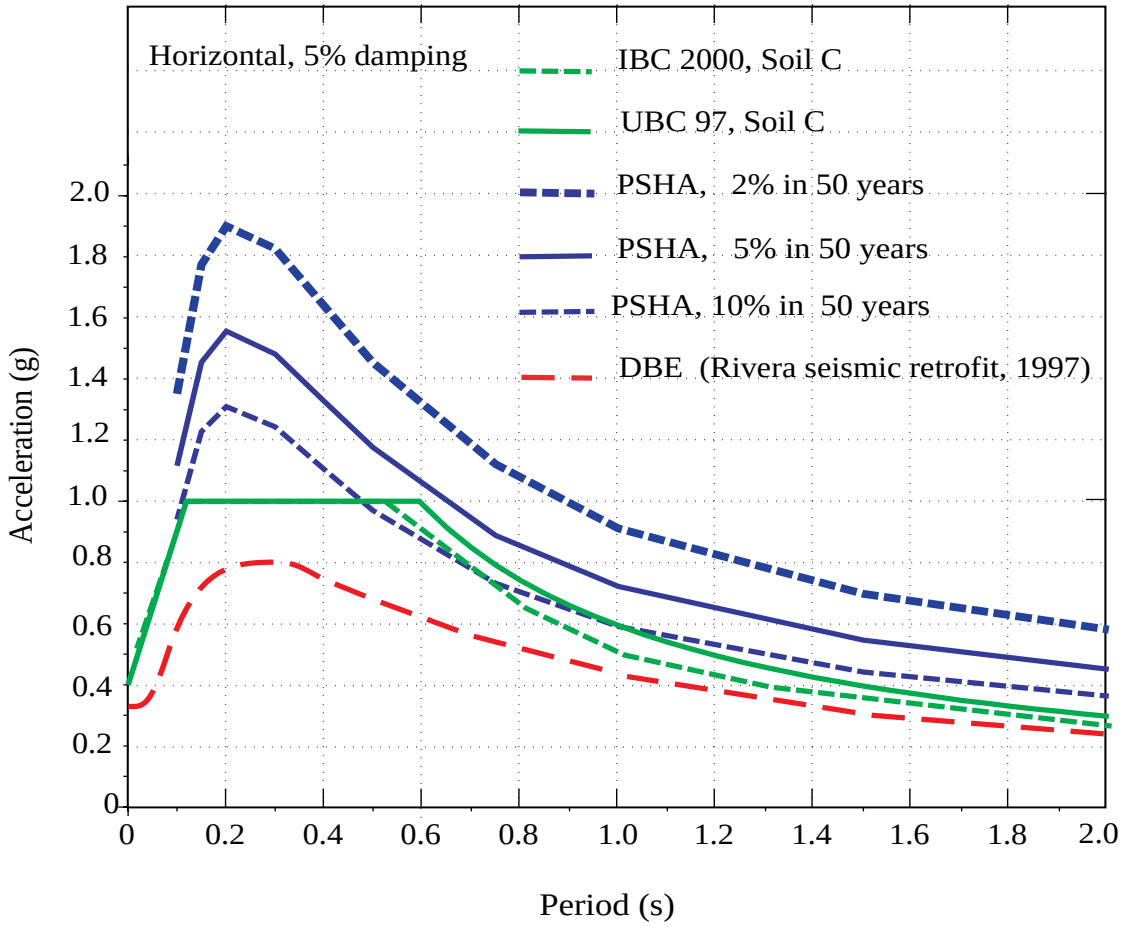

Figure 4.19 Comparison of various state-of-the-practice horizontal surface motions for UCR.

In turn, the CEP results of section 4.3.1 are compared to these state-of-the-practice estimates. Since the estimates of motions at the 3 UCR sites are fairly close to each other, the comparison with the state-of-the-practice is made for only one site, PL 16, in both horizontal directions (Figure 4.20). It is clear that the DBE used for the retrofit of Rivera library, and by extension for U.C. Riverside, is not adequate to represent the seismic exposure of the campus under any realistic assumption.

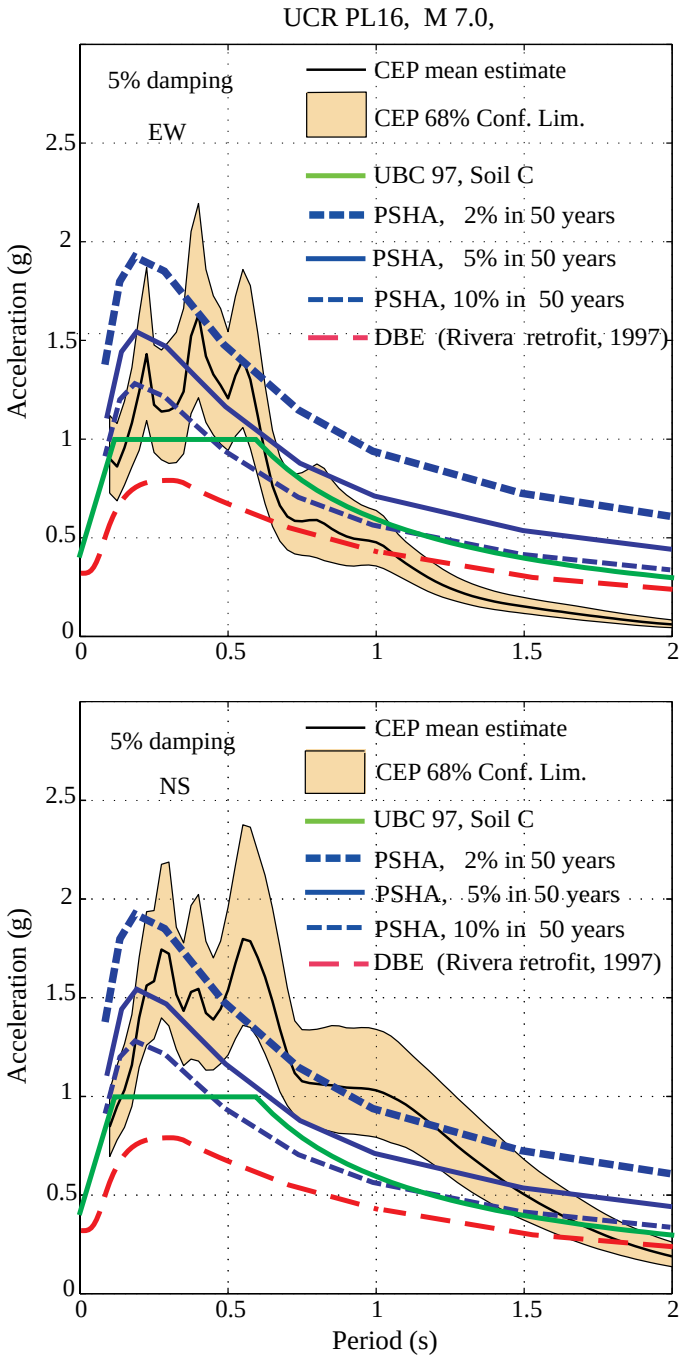

Figure 4.20 Comparison of CEP and state-of-the-practice surface motions for PL16 at UCR.

4.5 The CEP Estimates Versus Records from Recent M ~ 7 Earthquakes in California

The CEP estimated ground motions relate to a campus that is only 9 km away from fault segments capable of producing a M 7.0 earthquake. These estimates are significantly stronger than those currently adopted for the campus. In order to "calibrate" the severity of the estimated accelerations we show, for reference a comparison of the CEP estimates with acceleration spectra and acceleration time-histories corresponding to stations at somewhat comparable distances from 3 recent events of somewhat comparable magnitude in California (Figures 4.21 and 4.22). These comparisons should leave no doubt that the CEP-estimated motions are realistic.

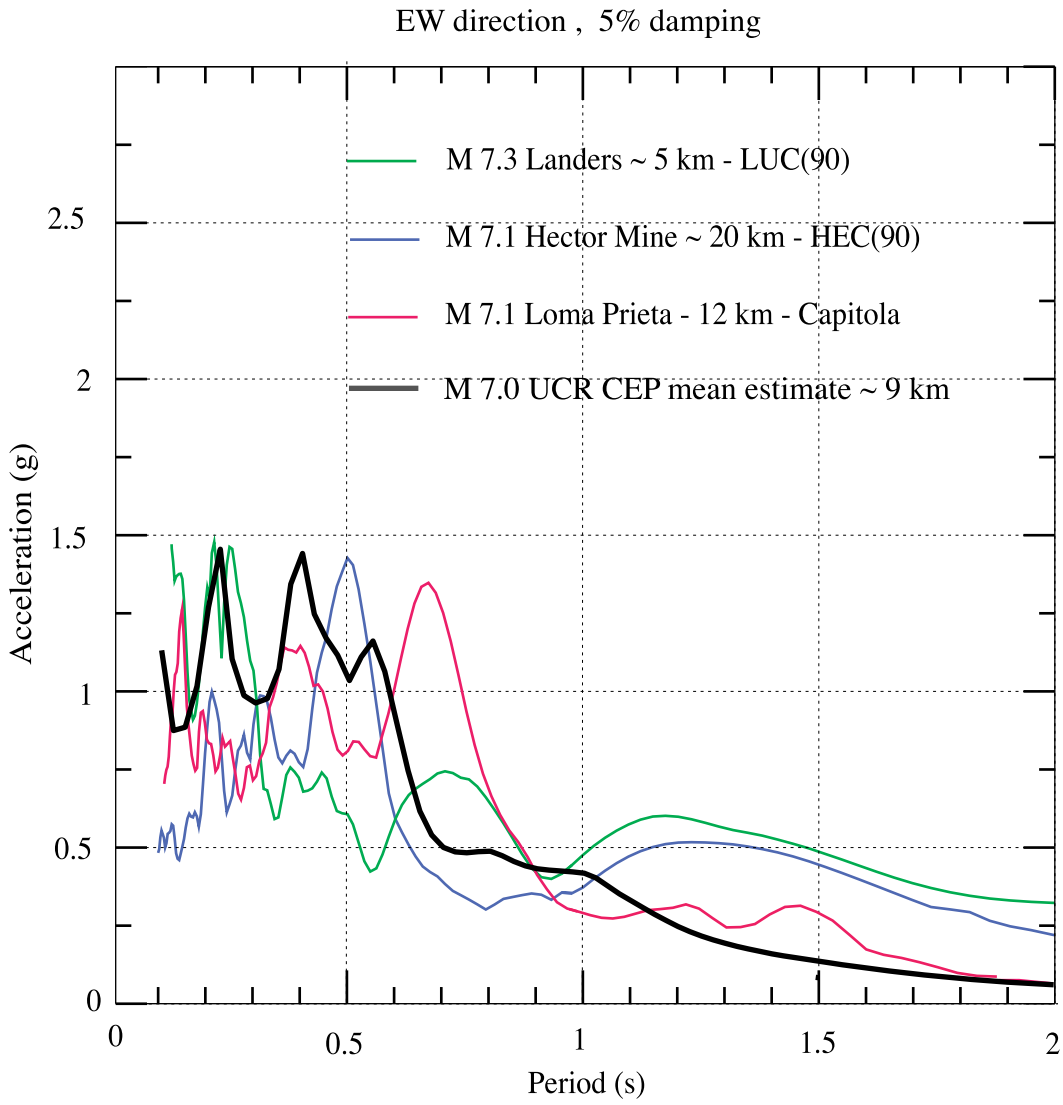

Figure 4.21 Horizontal acceleration spectra (EW) for recent M~7 earthquakes in California at ranges comparable to the distance from UCR to the San Jacinto fault, compared to the mean CEP.

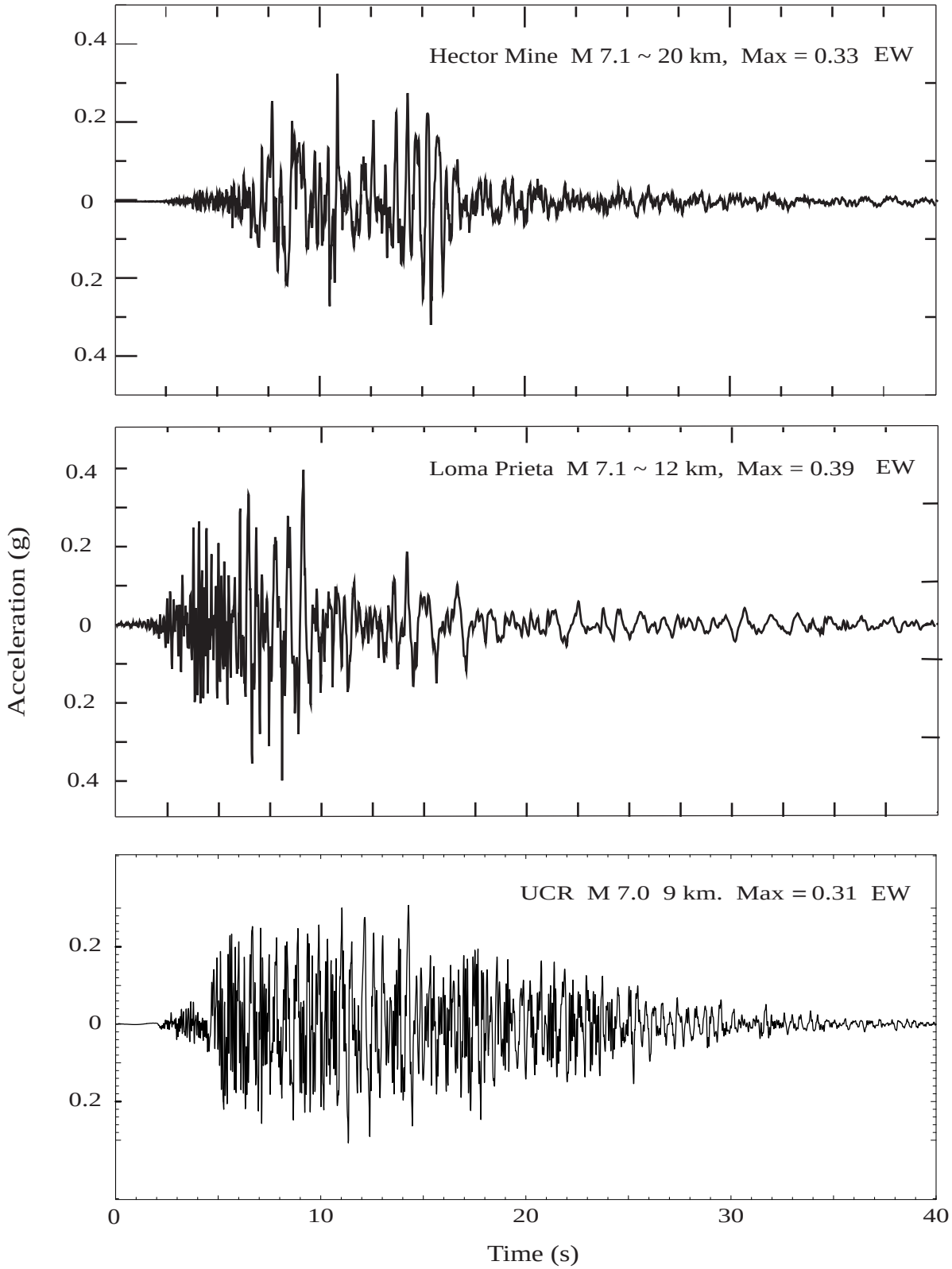

Figure 4.22 Horizontal acceleration time-histories (EW) for recent M~7 earthquakes in California, at ranges comparable to the distance from UCR to the San Jacinto fault compared to the mean CEP.

5.0 SUMMARY

This is the second report on the UC/CLC Campus Earthquake Program (CEP), concerning the estimation of exposure of the U.C. Riverside campus to strong earthquake motions (Phase 2 study). The first report (Phase 1), dated July 1999, covered the following topics:

- seismotectonic study of the Riverside region
- definition of causative faults threatening the UCR campus
- geophysical and geotechnical characterization of the Rivera library site
- installation of the new CEP seismic station
- and, initial acquisition of earthquake data on campus.

The main results of Phase 1 are summarized in the current report.

This document describes the studies which resulted in site-specific strong motion estimates for three sites on campus: Rivera library, Parking Lot 13 (PL 13), site of the future Physical Sciences 1 building, and Parking Lot 16 (PL 16) where the new Engineering Science 2 building is proposed for construction. The main elements of Phase 2 are:

- determining that a M 7.0 earthquake involving the San Jacinto Valley segment of the San Jacinto fault and a portion of the San Bernardino segment is the largest threat to the campus. Its recurrence interval is of the order of years.
- recording numerous small earthquakes from that portion of the fault at the new UCR seismic station and at five surface campus locations in 1999.
- Using the M 3.8 event recorded on March 22, 1999 as an empirical Green's functions (EGF) in scenario earthquake simulations which provided strong motion estimates (seismic syntheses) at depth of 89 m under the Rivera site, 69 m under the PL13 site, and 104 m under the PL 16 site; 120 such simulations were performed, each with the same seismic moment, but giving a broad range of motions which were analyzed for their mean and standard deviation.
- laboratory testing, at U.C. Berkeley and U.C. Los Angeles, of soil samples obtained from drilling at the UCR station site (Rivera library), to determine their response to earthquake-type loading.
- performing nonlinear soil dynamic calculations, using the soil properties determined in-situ and in the laboratory, to calculate the surface strong motions resulting from the seismic syntheses at depth.
- comparing these CEP-generated strong motion estimates to acceleration spectra based on the application of state-of-the-practice methods - the IBC 2000 code, the UBC 97 code, and

Probabilistic Seismic Hazard Analysis (PSHA). This comparison will be used to formulate design-basis spectra for future buildings and retrofits at UCR.

Because of the new, site-specific approach which the CEP studies represent, an extensive effort of validation is documented on several fronts:

- validation of the EGF methodology used in the seismic syntheses of strong motions at depth
- validation of the soil profiles used for the three UCR sites
- validation of the 1-D vertical seismic wave propagation assumption for the UCR sites
- validation of the nonlinear soil models used to obtain strong motions at the surface

The ever-growing database of strong earthquake records clearly demonstrates the potential for great variability of ground motions from site to site in a given earthquake. These variations are only reflected in a coarse way in the state-of-the-practice Probabilistic Seismic Hazard Analyses, which are rather generic. They are not either described by the simplified design spectra of the Building codes (UBC 97, IBC 2000). These shortcomings provide a strong justification for augmenting the state-of-the-practice estimates with site-specific studies such as done by the Campus Earthquake Program.

At UCR, the Phase 2 studies lead to the following important conclusions:

- the motions estimated at the three UCR sites are generally comparable. Because these sites have a fairly deep (more than 60 m) soil cover over the granite bedrock, it is expected that these CEP motions will be representative of those that could be expected at other campus locations where the soil cover is in excess of say 30 m. Motions at locations with shallower bedrock could be expected to be less severe because of a smaller amplification of bedrock motions by the soil profile.
- the horizontal motions corresponding to the mean CEP estimates are at least as strong as those corresponding to the PSHA estimates for a 950-year return period event. They are significantly higher (30 to 50%) than those corresponding to the UBC 1997 or the IBC 2000 spectra.
- the Design-Basis spectrum used in the retrofit of the Rivera library is considerably lower (a factor of 2) than the CEP mean estimates, and is substantially lower than the UBC, IBC, and 475-year return PSHA event.
- the + 1 sigma CEP estimates are comparable to the estimates from a 2375-year return period PSHA analysis.
- the motions estimated by the Campus Earthquake Program are very consistent with records from recent earthquakes of comparable magnitudes in California (Hector Mine, Landers, Loma Prieta).

These results should incite a re-examination of earthquake ground motion assumptions at UCR.

6.0 REFERENCES

Abrahamson, N. and Becker, A. Eds. (1999) "Proceedings of the MCEER Workshop on Ground Motion Methodologies for the Eastern United States", Technical Report MCEER-99-0016, State University of New York at Buffalo, NY.

Aki, K. (1967). "Scaling Law of Seismic Spectrum", J. Geophys. Res., v. 72, pp. 1217-1231.

Aki, K., and Richards, P.G. (1980) "Quantitative Seismology, Theory and Methods", 2 volumes, (W.H. Freeman and Company, San Francisco, CA).

Archuleta, R.J., Bonilla, L.F., and Lavallée, D. (1999), "Nonlinear Site Response Using Generalized Masing Rules Coupled with Pore Pressure", Proc. OECD-NRC Workshop on Engineering Characterization of Seismic Input, Brookhaven National Laboratory, NY, 32 pp, 1999.

Archuleta, R.J., Bonilla, L.F. and Lavallee, D. (2000a) "Nonlinearity in Observed and Computed Accelerograms", Proceeding of the 12th World Conference on Earthquake Engineering. Paper reference number 0338. (Aston Koedyk Ltd, 23b Westhaven Drive, Auckland, New Zealand).

Archuleta, R., Bonilla, F., Doroudian, M., Elgamal, A., Heuze, F., Hoehler, M., Lai, T., Lavallee, D., Liu, P-C., Martin, A., Riemer, M., Steidl, J., Vucetic, M., and Yang, Z. (2000b) "Strong Earthquake Motion Estimates for the UCSB Campus, and Related Response of the Engineering 1 Building", Lawrence Livermore National Laboratory, UCRL-ID-138641, 70 p., May.

Blake, T. (1999) " FRISKP 3.01b Brochure", T. Blake, 4568 Via Grande, Thousand Oaks, CA 91320.

Bonilla, L. F., Lavallée, D. and Archuleta, R.J. (1998) "Nonlinear Site Response: Laboratory modeling as a constraint for modeling accelerograms. Proceeding of the Second International Symposium on the Effects of Surface Geology on Seismic Motion, Vol. 2, pp 793-800, K. Irikura, K. Kudo H. Okada and T. Sasatani, Eds. (A.A. Balkema, Brookfield, VT).

Brune, J.N. (1970). "Tectonic Stress and the Spectra of Seismic Shear Waves from Earthquakes", J. Geophys. Res., v. 75, p. 5002.

Brune, J.N. (1971). Correction, J. Geophys. Res., v. 76, pp. 4997-5009.

Chen W-F., and Saleeb, A.F. (1982) "Constitutive Equations for Engineering Materials: Elasticity and Modeling", Volume 1, 580 pp., (John Wiley & Sons, New York).

CHJ Incorporated (1997) Letter Report to U.C. Riverside, from CHJ Inc., Coulton, CA, regarding the seismic retrofit of the Rivera library, including a Seismic Hazard Analysis from N. A.. Abrahamson to CHJ Inc.

Dan, K., Watanabe, T., Tanaka, T., and Sato, R. (1990) "Stability of Earthquake Ground Motions Synthesized by Using Different Small-Event Records as Empirical Green's Functions", Bulletin Seismological Soc. America, v. 80, pp. 1433-12455.

Doroudian, M., and Vucetic, M., (1995) "A Direct Simple Shear Device for Measuring Small Strain Behavior", ASTM Geotechnical Testing Journal, v. 18, n. 1, pp. 69-85.

Elgamal, A. W. (1991) "Shear Hysteretic Elasto-Plastic Earthquake Response of Soil Systems," Journal of Earthquake Engineering and Structural Dynamics, v. 20, n.4, pp. 371-387.

Elgamal, A. W. Parra, E., Yang, Z., Dobry, R., and Zeghal, M., (1999a) "Liquefaction Constitutive Model", Proc. Intl. Workshop on The Physics and Mechanics of Soil Liquefaction, Lade, P., and Yamamuro, J. A. Eds., Sept. 10-11, Baltimore, MD, 1998, Physics and Mechanics of Soil Liquefaction, (A.A. Balkema,, Brookfield, VT), pp. 269-279.

Elgamal, A.W., Yang, Z., Parra, E., and Dobry, R., (1999b) "Modeling of Liquefaction-Induced Shear Deformations", Second International Conference on Earthquake Geotechnical Engineering, Lisbon, Portugal, June 21-25, Earthquake Geotechnical Engineering, P. Seco e Pinto, Ed.,(A.A. Balkema, Brookfield, VT) pp. 895-900,

Hardin, B. O., (1965) "The Nature of Damping in Sands", ASCE J. Soil Mechanics and Foundation Division, v. 91, n. SM 1, pp. 63-97.

Hartzell, S. H. (1978). "Earthquake Aftershocks as Green's Functions", Geophysics Research. Letters, v. 5, pp. 1-4.

Hartzell, S. H., Liu, P.-C. and Mendoza, C. (1996) "The 1994 Northridge, California, Earthquake: Investigation of Rupture Velocity, Rise Time, and High-Frequency Radiation", J. Geophys. Res., v. 101, pp. 20091-20108.

Haskell, N.A. (1966) "Total Energy and Energy Spectral Density of Elastic Wave Radiation from Propagating Faults", Bulletin Seismological Soc. America, v. 56, pp. 125-140

Hutchings, L.J. (1991) " 'Prediction' of Strong Ground Motion for the 1989 Loma Prieta Earthquake, Using Empirical Green's Functions", Bulletin Seismological Soc. America, v. 81, n. 5, pp 1813-1857.

Hutchings, L.J., Jarpe, S.P., Kasameyer, P.W., and Foxall, W. (1996) "Synthetic Strong Ground Motions for Engineering Design, Utilizing Empirical Green's Functions", Lawrence Livermore National Laboratory Report UCRL-JC-123762, April.

International Conference of Building Officials (1998) "Maps of known active fault near-source zones in California and adjacent portions of Nevada", ISBN 1-58001-008-3, ICBO, Whittier, CA, February.

International Conference of Building Officials/ICBO (2000) "International Building Code 2000", ISBN 1-892395-25-8, 756 pp., March (ICBO, 5360 Workman Mill Road, Whittier, CA, 90601-2298).

Ishihara, K., (1996)" Soil Behaviour in Earthquake Geotechnics", 350 pp. (Clarendon Press, Oxford, U.K.).

Jackson, D.D. et al (1995) "Seismic Hazards in Southern California: Probable Earthquakes, 1994 to 2004", Bulletin Seismological Society of America, v. 85, pp 379-439.

Jarpe, S.P., and Kasameyer, P.K. (1996) "Validation of a Procedure for Calculating Broadband Strong-Motion Time-Histories With Empirical Green's Functions", Bulletin Seismological Soc. America, v. 86, pp. 1116-1129.

Kondner, R.L., and Zelasko, J.S. (1963) "A Hyperbolic Stress-Strain Formulation of Sands", Proc. 2nd Pan American Conference on Soil Mechanics and Foundation Engineering, Sao Paolo, Brazil, pp. 289-324.

Kramer, S. L., Von Laun, F-Y., and Sivaneswaran, N., (1992) "Strain-Controlled Variable-Frequency Cyclic Loading System for Soft Soils", ASTM Geotechnical Testing Journal, v. 15, pp. 264-270.

Kramer, S. L. (1996) "Geotechnical Earthquake Engineering", Prentice Hall, New Jersey, 653 pp.

Lawrence, B. (1999) "Site Characterization Studies for the U.C. Riverside Campus", Senior thesis, U.C. Riverside, 23 p.

Li, X.S., Wang, Z.L., and Chen, C.K. (1992) "SUMDES: A nonlinear procedure for response analysis of horizontally-layered sites subjected to multi-directional earthquake loading", Department of Civil Engineering, University of California, Davis, 86 p., March.

Masing, G. (1926) "Eigenspannungen und Verfestigung Beim Messing", Proc. 2nd Int. Congress Applied Mechanics, pp. 332-335.

Matesic, L., and Vucetic, M. (1998) "Results of Geotechnical Laboratory Tests on Soil Samples from the U.C. Riverside Campus", UCLA Department of Civil and Environmental Engineering, Report ENG-98-198, 208 p., Nov.

McCall, K. R. (1994) "Theoretical Study of Nonlinear Elastic Wave", J. Geophys. Res., v. 99, pp. 2591-2600.

Muravskii, G., and Frydman, S. (1998) "Site Response Analysis Using a Nonlinear Hysteretic Model", Soil Dynamics and Earthquake Engineering, v. 17, pp. 227-238.

Park, S.K., Elrick, S., and Funk, R. (1999), "Initial Source and Site Characterization Studies for the U.C. Riverside Campus", Lawrence Livermore National Laboratory Report, UCRL-ID-1346120, 73 p., July.

Pavic, R., Kollar, M.G., Bard, P-Y., and Lacave-Lachet, C. (2000) "Ground Motion Prediction with the Empirical Green's Function Technique: An Assessment of Uncertainties and Confidence Level", J. of Seismology, v. 4, pp. 59-77

Petersen, M. et al. (1996) "Probabilistic Seismic Hazard Assessment for the State of California",California Department of Conservation, Division of Mines and Geology, Open-file Report 96-08. Also available as U.S. Geological Survey Open-file Report 96-706.

Pitilakis, K.D. and Anastasiadis, A.J. (1998) "Soil and Site Characterization for Seismic Response Analysis", Proceedings Eleventh European Conference on Earthquake Engineering, Sept. 6-11, Paris, France, pp. 65-90 (A.A. Balkema, Brookfield, VT).

Pyke, R., (1979) "Nonlinear Soil Model for Irregular Cyclic Loadings", ASCE J. of the Geotechnical Engineering Div., v. 105, n. 6, pp. 715-726.

Riemer, M., and Abu-Safaqh, O., (1999) "Large Strain Triaxial Testing of Soil Samples from U.C. Riverside", University of California at Berkeley, Department of Civil Engineering, Report, March.

Tumarkin, A.G., and Archuleta, R.J. (1994) "Empirical Ground Motion Prediction", Annali di Geofisica, v. 37, n. 6, pp. 1691-1720.

Vucetic, M. (1990) "Normalized Behavior of Clay Under Irregular Cyclic Loading", Canadian Geotechnical Journal, v. 27, pp. 29-46.

Wu, F. T. (1978) "Prediction of Strong Ground Motion Using Small Earthquakes", in Proc. 2nd International Microzonation Conference, San Francisco, (Nat. Science Found.), v. 2, pp. 701-704.

Xu, H., Day, S.M., and Minster, J.B. (1998) "Model for Nonlinear Wave Propagation Derived from Rock Hysteresis Measurements", J. Geophys. Res., v. 103, pp. 29915-29929, 1998.

Yoshida, N. and Iai, S. (1998) "Nonlinear Site Response and its Evaluation and Prediction", Proceeding of the Second International Symposium on the Effects of Surface Geology on Seismic Motion, v. 1, A.A. Balkema, Brookfield, VT, pp. 71-90.

7.0 ACKNOWLEDGMENTS

These studies were funded from several sources: the University of California Senior Vice-President Business and Finance, Wayne Kennedy, the University of California Office of Research directed by Dr. Robert Shelton, the Office of the Vice-Chancellor Administration at U.C. Riverside, C. Michael Webster., and the University Relations Program at the Lawrence Livermore National Laboratory, previously headed by Dr. Claire Max and currently by Dr. Harry Radousky. We express our deep appreciation to all for their continued support.